DAΦNE TECHNICAL NOTE

INFN - LNF, Accelerator Division

Frascati, Dec. 2, 1991

Note: **L-4**

DAΦNE LATTICE UPDATE

M.E. Biagini, S. Guiducci, M.R. Masullo, G. Vignola

1. INTRODUCTION

An improved version of the DAΦNE high emittance lattice is presented. The basic criteria of the design are the same as in L-1 [1], but the structure of the arcs has been slightly modified in order to achieve a better β separation at the location of the chromaticity correcting sextupoles, and a higher momentum compaction. Moreover, a new working point has been chosen in order to improve the dynamic aperture and a more realistic model for the wiggler magnet has been adopted. Let us remind that each ring is divided in a long half and a short half, for simplicity called hereafter *Long* and *Short*.

2. THE STORAGE RINGS

The layout of the two rings is shown in **Fig. 2.1**. In the following we summarize the main differences with respect to the previous structure:

a) The two arc dipoles are of a different type: the first one nearer to the IP is a sector type dipole, while the second is a rectangular type *(parallel end)* one. The bending angle is however the same for both.

b) A more realistic model than the rectangular one has been adopted for the wiggler magnet. Each pole is divided in three pieces: a central part with the maximum field value $B=B_0$ and two sidepieces with $B=B_0/2$ and length equal to twice the gap. the self-β in the vertical plane is ~ 1.2 m.

c) Small changes in the quadrupole arrangement have also been done:
   - a quadrupole has been added in the matching section between the IR and the first dipole;
   - only one quadrupole, instead of two has been left between the wiggler and second dipole;
   - the number of quadrupoles in the injection and RF straight sections has been increased by one (respectively from 7 to 8 and from 6 to 7).

In summary, the total number of quadrupoles is now 39 for each ring plus 12 for the low-β insertions. The circumference has been thus slightly increased (97.69 m). In **Tables 2.I** and **2.II** the output of the LEDA code with the list of the elements, respectively for half of the *Long* and *Short* sections, is given. The single ring parameters are listed in **Table 2.III**.

Table 2.I

DAFNE LONG

ENERGY (MeV)	510.0
TOTAL BENDING ANGLE(deg)	389.187
TOTAL LENGTH (m)	51.3315559
TUNES: QX - QZ	2.680 - 2.260

	TYPE	LENGTH(m)	K2(m-2)	B'(T/m) - B"(T/m2)	RADIUS(m)		x(mm)	x'(mrad)
*	I.P.						0.0	10.0
1	O	0.450					4.500225	"
2	QI1	0.18	4.35	7.40			5.862052	5.86205
3	O	0.13					6.706883	"
4	QI2	0.34	-7.00	11.90			11.881470	26.60213
5	O	0.13					15.340970	"
6	QI3	0.28	3.95	6.72			20.096300	6.483416
7	O	3.49					42.723900	"
8	SM	1.45			-10.	==> SPLITTER		
9	O	1.1						
10	QL10	0.3	0.837021	1.42				
11	O	0.4						
12	QL9	0.3	-1.405321	2.39				
13	O	0.3						
14	SDL4	0.2	0.30	2.60				
15	O	0.2						
16	QL8	0.3	0.592361	1.01				
17	O	0.6						
18	BSS	1.2057			1.40012	==> SECTOR		
19	O	0.6						
20	QL7	0	-2.137196	3.63				
21	O	0.2						
22	SDL3	0.2	4.60	39.10				
23	O	0.2						
24	QL6	0.3	2.574517	4.53				
25	O	0.6						
26	WIG	B=1.8 T - 2x20 HALF poles + 5x32 FULL poles ==> 2. m length						
27	O	0.2						
28	SFL2	0.2	-2.00	17.00				
29	O	0.2						
30	QL5	0.3	1.82198	3.10				
31	O	0.6						
32	BSP	1.2057			1.40012	==> PARALLEL		
33	O	0.3						
34	SDL1	0.2	1.00	8.50				
35	O	0.9						
36	QL4	0.3	-1.130138	1.92				
37	O	0.5						
38	QL3	0.3	3.971584	6.75				
39	O	1.9						
40	QL2	0.3	-2.64373074	4.49				
41	O	0.5						
42	QL1	0.3	2.354521	4.00				
43	O	1.7						

************* SIMMETRICALLY REFLECTED **************

Table 2.II

DAFNE SHORT

ENERGY (MeV)	510.0
TOTAL BENDING ANGLE(deg)	354.468
TOTAL LENGTH (m)	46.3587547
TUNES: QX - QZ	2.19 - 2.59

	TYPE	LENGTH(m)	K2(m-2)	B'(T/m) - B"(T/m2)	RADIUS(m)	x(mm)	x'(mrad)
*	I.P.					0.0	10.0
1	O	0.450				4.500225	"
2	QI1	0.18	4.35	7.40		5.862052	5.86205
3	O	0.13				6.706883	"
4	QI2	0.34	-7.00	11.90		11.881470	26.60213
5	O	0.13				15.340970	"
6	QI3	0.28	3.95	6.72		20.096300	6.483416
7	O	3.49				42.723900	"
8	SM	1.45			10.	==> SPLITTER	
9	O	1.1					
10	QS10	0.3	1.345122	2.29			
11	O	0.4					
12	QS9	0.3	-2.053632	3.49			
13	O	0.7					
14	QS8	0.3	1.046177	1.78			
15	O	0.6					
16	BSS	0.9936			1.40012	==> SECTOR	
17	O	0.6					
18	QS7	0.3	-2.102922	3.57			
19	O	0.2					
20	SDS2	0.2	12.65	107.5			
21	O	0.2					
22	QS6	0.3	2.427586	4.13			
23	O	0.6					
24	WIG	B=1.8 T - 2x20 HALF poles + 5x32 FULL poles ==> 2. m length					
25	O	0.2					
26	SFS1	0.2	-3.4	28.9			
27	O	0.2					
28	QS5	0.3	1.380068	2.35			
29	O	0.6					
30	BSP	0.9936			1.40012	==> PARALLEL	
31	O	0.6					
32	QS4	0.3	-1.956182	3.33			
33	O	0.4					
34	QS3	0.3	2.411142	4.10			
35	O	2.40779943					
36	QS2	0.3	-3.084062	5.24			
37	O	0.66					
38	QS1	0.17	3.981575	6.77			

************ SIMMETRICALLY REFLECTED **************

Table 2.III - DAΦNE single ring parameters list

Energy (MeV)		510
Circumference (m)		97.69
Dipole bending radius (m)		1.400
Wiggler bending radius(m)		0.94
Wiggler length (m)		2.0
Wiggler period (m)		.66
Horizontal β-tune		4.87
Vertical β-tune		4.85
Natural chromaticities:	Horizontal	-6.9
	Vertical	-16.9
Momentum compaction		.017
I_2 (m^{-1})		9.76
I_3 (m^{-2})		8.07
Energy loss/turn (KeV):	Bend.magnets	4.27
	Wigglers	4.96
	Total	9.3
Damping times (msec):	τ_s	17.8
	τ_x	36.02
	τ_y	35.73
β_y @ IP (m)		.045
β_x @ IP (m)		4.5
σ_y @ IP (mm)		.021
σ_x @ IP (mm)		2.11
κ		.01
Emittance (m-rad)		10^{-6}
Natural relative rms energy spread	σ_p*	$3.97\ 10^{-4}$
Natural bunch length σ_z (cm)		.81
Anomalous bunch length σ_z (cm)		3.0
Crossing half angle (mrad)		10.0
RF frequency (MHz)		368.25
Harmonic number		120
Number of bunches		1 ÷ 120
Maximum number of particle/bunch		9.10^{10}
Maximum bunch peak current (A)		57
Maximum average current/bunch (mA)		44
Maximum total average current (A)		5.3
Maximum synchrotron power/beam (KW)		49
V_{RF} (KV)	@ Z/n = 2 Ω	254
	@ Z/n = 1 Ω	127
Parasitic losses @ σ_z = 3 cm (KeV/Ω)**		7

* $\sigma_p \sim 10^{-3}$ @ 44 mA/bunch

** L. Palumbo, M. Serio: "Energy Loss due to the Broad-band Impedance in DAΦNE", DAΦNE Technical Note G-7, Sept. 2, 1991.

Different lattices have been studied, in order to optimize the lattice performances in lifetime, injection and chromaticity correction. They all show good performances, and a detailed description is given in the Appendix. The lattice chosen presents flexibility, a high momentum compaction, a larger dynamic aperture - especially for off-energy particles - and finally a more homogeneous structure between the *Short* and *Long*.

3. BEAM OPTICS

The optical functions of the ring, for half of the *Short* and *Long* respectively, are shown in **Figs. 3.1** and **3.2**, and the relative MAD outputs are given in **Tables 3.I** and **3.II**.

The working point, different from the solution presented in L-1, is below the integer in both planes: this results in a larger dynamic aperture. A work by M. Bassetti, based on the analysis of experimental data, is in progress on the influence of the working point choice on the maximum achievable tune shift.

Table 3.I

DAFNE - NUX=4.87, NUY=4.85 - DAF6 (OCTOBER '91)
Linear lattice functions for beam line: HALF-SHORT

ELEMENT SEQUENCE				HORIZONTAL							VERTICAL						
pos. no.	element name	occ. no.	dist [m]	betax (m)	alfax (1)	mux (2pi)	x(co) (mm)	px(co) [.001]	Dx (m)	Dpx (1)	betay (m)	alfay (1)	muy (2pi)	y(co) (mm)	py(co) [.001]	Dy (m)	Dpy (1)
1	IP2	1	0.000	4.500	0.000	0.000	0.000	0.000	0.000	0.000	0.045	0.000	0.000	0.000	0.000	0.000	0.000
2	DI1	1	0.450	4.545	-0.100	0.016	0.000	0.000	0.000	0.000	4.545	-10.000	0.234	0.000	0.000	0.000	0.000
3	QI1	1	0.630	3.974	3.124	0.022	0.000	0.000	0.000	0.000	9.919	-21.244	0.239	0.000	0.000	0.000	0.000
4	DI2	1	0.760	3.207	2.772	0.028	0.000	0.000	0.000	0.000	16.213	-27.172	0.240	0.000	0.000	0.000	0.000
5	QI2	1	1.100	3.909	-5.368	0.046	0.000	0.000	0.000	0.000	20.270	18.648	0.243	0.000	0.000	0.000	0.000
6	DI3	1	1.230	5.435	-6.359	0.050	0.000	0.000	0.000	0.000	15.710	16.410	0.244	0.000	0.000	0.000	0.000
7	QI3	1	1.510	7.327	0.313	0.057	0.000	0.000	0.000	0.000	11.385	0.601	0.247	0.000	0.000	0.000	0.000
8	DI4	1	5.000	6.969	-0.210	0.138	0.000	0.000	0.000	0.000	8.648	0.183	0.305	0.000	0.000	0.000	0.000
9	SM	1	6.450	7.737	-0.316	0.170	0.000	0.000	0.105	0.144	8.367	0.010	0.332	0.000	0.000	0.000	0.000
10	DS16	1	7.550	8.604	-0.472	0.191	0.000	0.000	0.264	0.144	8.490	-0.121	0.353	0.000	0.000	0.000	0.000
11	QS10	1	7.850	7.878	2.797	0.197	0.000	0.000	0.291	0.031	9.650	-3.900	0.358	0.000	0.000	0.000	0.000
12	DS15	1	8.250	5.819	2.349	0.206	0.000	0.000	0.303	0.031	13.038	-4.572	0.364	0.000	0.000	0.000	0.000
13	QS9	1	8.550	5.480	-1.150	0.215	0.000	0.000	0.341	0.227	13.333	3.651	0.367	0.000	0.000	0.000	0.000
14	DS14	1	8.750	5.957	-1.235	0.221	0.000	0.000	0.387	0.227	11.915	3.436	0.370	0.000	0.000	0.000	0.000
15	DS14	2	8.950	6.468	-1.320	0.226	0.000	0.000	0.432	0.227	10.584	3.221	0.373	0.000	0.000	0.000	0.000
16	DS13	1	9.250	7.299	-1.447	0.233	0.000	0.000	0.500	0.227	8.747	2.899	0.378	0.000	0.000	0.000	0.000
17	QS8	1	9.550	7.485	0.847	0.239	0.000	0.000	0.544	0.062	7.847	0.198	0.383	0.000	0.000	0.000	0.000
18	DS12	1	10.150	6.551	0.709	0.253	0.000	0.000	0.581	0.062	7.657	0.119	0.396	0.000	0.000	0.000	0.000
19	BSS	1	11.144	2.979	2.261	0.286	0.000	0.000	0.835	0.428	7.552	-0.013	0.417	0.000	0.000	0.000	0.000
20	DS11	1	11.744	1.004	1.030	0.342	0.000	0.000	1.092	0.428	7.615	-0.093	0.429	0.000	0.000	0.000	0.000
21	QS7	1	12.044	0.704	0.032	0.402	0.000	0.000	1.330	1.180	6.322	4.126	0.436	0.000	0.000	0.000	0.000
22	DS10	1	12.244	0.748	-0.252	0.447	0.000	0.000	1.566	1.180	4.786	3.556	0.442	0.000	0.000	0.000	0.000
23	SDS2	1	12.444	0.906	-0.536	0.486	0.000	0.000	1.802	1.180	3.478	2.986	0.450	0.000	0.000	0.000	0.000
24	DS9	1	12.644	1.178	-0.820	0.517	0.000	0.000	2.038	1.180	2.398	2.416	0.461	0.000	0.000	0.000	0.000
25	QS6	1	12.944	1.481	-0.116	0.552	0.000	0.000	2.160	-0.377	1.567	0.553	0.486	0.000	0.000	0.000	0.000
26	DS8	1	13.544	1.867	-0.527	0.610	0.000	0.000	1.934	-0.377	1.203	0.053	0.558	0.000	0.000	0.000	0.000
27	WIG	1	15.548	6.711	-1.896	0.706	0.000	0.000	1.179	-0.378	1.203	-0.053	0.824	0.000	0.000	0.000	0.000
28	DS7	1	15.748	7.497	-2.032	0.711	0.000	0.000	1.103	-0.378	1.258	-0.220	0.850	0.000	0.000	0.000	0.000
29	SFS1	1	15.948	8.337	-2.169	0.715	0.000	0.000	1.028	-0.378	1.379	-0.386	0.875	0.000	0.000	0.000	0.000
30	DS6	1	16.148	9.232	-2.306	0.718	0.000	0.000	0.952	-0.378	1.567	-0.553	0.896	0.000	0.000	0.000	0.000
31	QS5	1	16.448	9.463	1.568	0.723	0.000	0.000	0.783	-0.741	2.208	-1.671	0.923	0.000	0.000	0.000	0.000
32	DS5	1	17.048	7.713	1.349	0.734	0.000	0.000	0.338	-0.741	4.832	-2.702	0.952	0.000	0.000	0.000	0.000
33	BSP	1	18.042	5.556	1.015	0.757	0.000	0.000	0.000	0.000	8.279	0.145	0.977	0.000	0.000	0.000	0.000
34	DS4	1	18.642	4.469	0.796	0.776	0.000	0.000	0.000	0.000	8.150	0.071	0.989	0.000	0.000	0.000	0.000
35	QS4	1	18.942	4.802	-1.971	0.786	0.000	0.000	0.000	0.000	6.770	4.255	0.995	0.000	0.000	0.000	0.000
36	DS3	1	19.342	6.542	-2.378	0.798	0.000	0.000	0.000	0.000	3.817	3.126	1.008	0.000	0.000	0.000	0.000
37	QS3	1	19.642	6.536	2.395	0.805	0.000	0.000	0.000	0.000	2.821	0.431	1.023	0.000	0.000	0.000	0.000
38	DS2	1	22.049	0.978	-0.086	1.006	0.000	0.000	0.000	0.000	3.182	-0.581	1.171	0.000	0.000	0.000	0.000
39	QS2	1	22.349	1.439	-1.590	1.048	0.000	0.000	0.000	0.000	2.699	2.037	1.187	0.000	0.000	0.000	0.000
40	DS1	1	23.009	4.606	-3.208	1.090	0.000	0.000	0.000	0.000	0.841	0.778	1.259	0.000	0.000	0.000	0.000
41	QS1	1	23.179	5.173	0.000	1.095	0.000	0.000	0.000	0.000	0.714	0.000	1.295	0.000	0.000	0.000	0.000
42	SYMS	1	23.179	5.173	0.000	1.095	0.000	0.000	0.000	0.000	0.714	0.000	1.295	0.000	0.000	0.000	0.000

total length =	23.179377	mux	= 1.095000	muy	= 1.295000
delta(s) =	0.000000 mm	dmux	= -1.215060	dmuy	= -2.320021
		betax(max)	= 9.463277	betay(max)	= 20.269571
		Dx(max)	= 2.160371	Dy(max)	= 0.000000
		Dx(r.m.s.)	= 1.137675	Dy(r.m.s.)	= 0.000000

Table 3.II

DAFNE - MUX=4.87, MUY=4.85 - DAF6 (OCTOBER '91)
Linear lattice functions for beam line: HALF-LONG

ELEMENT SEQUENCE				HORIZONTAL							VERTICAL						
pos. no.	element name	occ. no.	dist [m]	betax [m]	alfax [1]	mux [2pi]	x(co) [mm]	px(co) [.001]	Dx [m]	Dpx [1]	betay [m]	alfay [1]	muy [2pi]	y(co) [mm]	py(co) [.001]	Dy [m]	Dpy [1]
1	IP1	1	0.000	4.500	0.000	0.000	0.000	0.000	0.000	0.000	0.045	0.000	0.000	0.000	0.000	0.000	0.000
2	DI1	1	0.450	4.545	-0.100	0.016	0.000	0.000	0.000	0.000	4.545	-10.000	0.234	0.000	0.000	0.000	0.000
3	QI1	1	0.630	3.974	3.124	0.022	0.000	0.000	0.000	0.000	9.919	-21.244	0.239	0.000	0.000	0.000	0.000
4	DI2	1	0.760	3.207	2.772	0.028	0.000	0.000	0.000	0.000	16.213	-27.172	0.240	0.000	0.000	0.000	0.000
5	QI2	1	1.100	3.909	-5.368	0.046	0.000	0.000	0.000	0.000	20.270	18.648	0.243	0.000	0.000	0.000	0.000
6	DI3	1	1.230	5.435	-6.359	0.050	0.000	0.000	0.000	0.000	15.710	16.410	0.244	0.000	0.000	0.000	0.000
7	QI3	1	1.510	7.327	0.313	0.057	0.000	0.000	0.000	0.000	11.385	0.601	0.247	0.000	0.000	0.000	0.000
8	DI4	1	5.000	6.969	-0.210	0.138	0.000	0.000	0.000	0.000	8.648	0.183	0.305	0.000	0.000	0.000	0.000
9	SML	1	6.450	7.737	-0.316	0.170	0.000	0.000	-0.105	-0.144	8.367	0.010	0.332	0.000	0.000	0.000	0.000
10	DL18	1	7.550	8.604	-0.472	0.191	0.000	0.000	-0.264	-0.144	8.490	-0.121	0.353	0.000	0.000	0.000	0.000
11	QL10	1	7.850	8.254	1.610	0.197	0.000	0.000	-0.297	-0.074	9.233	-2.418	0.358	0.000	0.000	0.000	0.000
12	DL17	1	8.250	7.036	1.436	0.205	0.000	0.000	-0.326	-0.074	11.286	-2.715	0.364	0.000	0.000	0.000	0.000
13	QL9	1	8.550	7.068	-1.550	0.212	0.000	0.000	-0.370	-0.219	11.477	2.106	0.369	0.000	0.000	0.000	0.000
14	DL16	1	9.250	9.474	-1.886	0.226	0.000	0.000	-0.523	-0.219	8.760	1.775	0.380	0.000	0.000	0.000	0.000
15	QL8	1	9.550	10.112	-0.204	0.230	0.000	0.000	-0.574	-0.121	8.176	0.207	0.385	0.000	0.000	0.000	0.000
16	DL15	1	9.750	10.198	-0.224	0.234	0.000	0.000	-0.598	-0.121	8.098	0.182	0.389	0.000	0.000	0.000	0.000
17	SDL4	1	9.950	10.291	-0.245	0.237	0.000	0.000	-0.622	-0.121	8.031	0.156	0.393	0.000	0.000	0.000	0.000
18	DL14	1	10.150	10.394	-0.266	0.240	0.000	0.000	-0.647	-0.121	7.973	0.131	0.397	0.000	0.000	0.000	0.000
19	BLS	1	11.356	4.896	3.638	0.264	0.000	0.000	-0.062	1.030	7.843	-0.023	0.422	0.000	0.000	0.000	0.000
20	DL13	1	11.956	1.577	1.894	0.298	0.000	0.000	0.556	1.030	7.917	-0.100	0.434	0.000	0.000	0.000	0.000
21	QL7	1	12.256	0.892	0.536	0.340	0.000	0.000	0.930	1.499	6.552	4.352	0.440	0.000	0.000	0.000	0.000
22	DL12	1	12.456	0.736	0.247	0.380	0.000	0.000	1.229	1.499	4.933	3.744	0.446	0.000	0.000	0.000	0.000
23	SDL3	1	12.656	0.694	-0.042	0.425	0.000	0.000	1.529	1.499	3.557	3.135	0.453	0.000	0.000	0.000	0.000
24	DL11	1	12.856	0.769	-0.330	0.469	0.000	0.000	1.829	1.499	2.425	2.526	0.464	0.000	0.000	0.000	0.000
25	QL6	1	13.156	0.893	-0.051	0.526	0.000	0.000	2.054	-0.030	1.567	0.553	0.490	0.000	0.000	0.000	0.000
26	DL10	1	13.756	1.359	-0.725	0.618	0.000	0.000	2.036	-0.030	1.203	0.053	0.562	0.000	0.000	0.000	0.000
27	WIG	1	15.760	8.751	-2.971	0.716	0.000	0.000	1.974	-0.031	1.203	-0.053	0.828	0.000	0.000	0.000	0.000
28	DL9	1	15.960	9.984	-3.196	0.719	0.000	0.000	1.968	-0.031	1.257	-0.220	0.854	0.000	0.000	0.000	0.000
29	SFL2	1	16.160	11.307	-3.420	0.722	0.000	0.000	1.962	-0.031	1.379	-0.386	0.878	0.000	0.000	0.000	0.000
30	DL8	1	16.360	12.720	-3.645	0.725	0.000	0.000	1.956	-0.031	1.567	-0.553	0.900	0.000	0.000	0.000	0.000
31	QL5	1	16.660	12.797	3.403	0.729	0.000	0.000	1.788	-1.069	2.286	-1.976	0.926	0.000	0.000	0.000	0.000
32	DL7	1	17.260	9.068	2.813	0.738	0.000	0.000	1.147	-1.069	5.430	-3.263	0.953	0.000	0.000	0.000	0.000
33	BLP	1	18.466	4.201	1.769	0.765	0.000	0.000	0.500	-0.150	9.859	1.043	0.980	0.000	0.000	0.000	0.000
34	DL6	1	18.866	2.943	1.376	0.783	0.000	0.000	0.440	-0.150	9.058	0.958	0.986	0.000	0.000	0.000	0.000
35	SDL1	1	19.066	2.432	1.179	0.795	0.000	0.000	0.410	-0.150	8.683	0.916	0.990	0.000	0.000	0.000	0.000
36	DL5	1	19.866	1.175	0.393	0.874	0.000	0.000	0.290	-0.150	7.354	0.746	1.006	0.000	0.000	0.000	0.000
37	QL4	1	20.166	1.138	-0.265	0.916	0.000	0.000	0.259	-0.058	6.231	2.868	1.013	0.000	0.000	0.000	0.000
38	DL4	1	20.666	1.638	-0.736	0.976	0.000	0.000	0.230	-0.058	3.733	2.128	1.029	0.000	0.000	0.000	0.000
39	QL3	1	20.966	1.538	1.030	1.004	0.000	0.000	0.174	-0.306	3.781	-2.306	1.043	0.000	0.000	0.000	0.000
40	DL3	1	22.866	2.461	-1.516	1.289	0.000	0.000	-0.407	-0.306	18.573	-5.480	1.079	0.000	0.000	0.000	0.000
41	QL2	1	23.166	4.283	-5.031	1.304	0.000	0.000	-0.552	-0.678	17.435	8.968	1.082	0.000	0.000	0.000	0.000
42	DL2	1	23.666	10.850	-8.103	1.316	0.000	0.000	-0.891	-0.678	9.635	6.633	1.088	0.000	0.000	0.000	0.000
43	QL1	1	23.966	13.427	0.129	1.320	0.000	0.000	-0.995	0.000	7.709	0.232	1.094	0.000	0.000	0.000	0.000
44	DL1	1	25.666	13.208	0.000	1.340	0.000	0.000	-0.995	0.000	7.314	0.000	1.130	0.000	0.000	0.000	0.000
45	SYML	1	25.666	13.208	0.000	1.340	0.000	0.000	-0.995	0.000	7.314	0.000	1.130	0.000	0.000	0.000	0.000

total length =	25.665778	mux =	1.340020	muy =	1.130000
delta(s) =	0.000000 mm	dmux =	-1.413926	dmuy =	-4.843128
		betax(max) =	13.427196	betay(max) =	20.269571
		Dx(max) =	2.053599	Dy(max) =	0.000000
		Dx(r.m.s.) =	1.400456	Dy(r.m.s.) =	0.000000

The total chromaticity is nearly the same as in L-1:

$$\xi_x = -6.9 \ , \quad \xi_y = -16.9$$

The **low-β insertion** is essentially the same as in L-1, with minor modifications of the lengths and of quadrupole strengths. The calculations are performed using on axis quadrupoles for the triplet, therefore the dispersion is zero in the IR. Taking into account the displacement of the quadrupole axis gives a negative dispersion of a few centimetres.

In **Fig. 3.3** the half separation Δx between the two beams in the low-β insertion and the horizontal and vertical beam sizes in the same region are plotted.

In **Table 3.III**, the ascissa s, Δx, β_x, β_y and the linear tune shifts ξ_x and ξ_y, with respect to the maximum ξ = .04 at the IP, are shown, computed at the parasitic crossing points for a frequency of 368.25 MHz (h=120).

Table 3.III

s (m)	Δ**x** (mm)	β_x (m)	β_y (m)	ξ_x^p	ξ_y^p
.4	4.0	4.54	3.56	.0028	.0022
.8	7.0	3.02	18.26	.0006	.0037
1.2	14.5	5.06	16.71	.0002	.0008
1.6	20.7	7.27	11.28	.0002	.0003

In **Table 3.IV** the maximum allowable diameter, the horizontal beam size and the half separation Δx between the beam centers are given at the edges of each quadrupole.

Table 3.IV

	s (m)	**Øout** (mm)	σ_x (mm)	Δ_x (mm)
Q1	.45	134	2.13	4.50
	.63	187	1.99	5.94
Q2	.76	226	1.79	6.71
	1.10	326	1.98	11.9
Q3	1.23	364	2.33	15.3
	1.51	448	2.71	20.1
Splitter	5.0	—	2.64	42.7

In the **achromat**, the D quadrupole near to the second bending magnet has been eliminated and the vertical focusing is given by the parallel faces of the dipole. This gives a very good separation of the β-functions at the sextupole locations.

Moreover the lattice has been modified in order to have the optical functions of the *Short* and *Long* as similar as possible, and therefore to put the F and D sextupoles respectively in the same locations. This is one reason for having a third quadrupole in the matching section and the same angle for the bending magnets of each arc.

The main modification for the ***Long*** **straight section** is the decision to allow a non-vanishing, negative dispersion in the injection region, in order to obtain a higher value of the momentum compaction. Increasing the dispersion to nearly one meter, the value of the momentum compaction is changed from .0068 to .017. This is an example of the lattice flexibility: in fact the value of the momentum compaction plays an important role on considerations on the instability thresholds and on the RF parameters.

Due to the low value of the energy spread of the beam coming from the accumulator (~10^{-3}) the injection efficiency should not be affected by a dispersion of about one meter at the injection point.

The horizontal betatron phase in the *Long* is related to the value of the dispersion in the injection section, therefore to easily tune the betatron wavenumber of the ring in both planes a quadrupole has been added in the *Short* (which still has zero dispersion in the RF straight section).

4. THE DYNAMIC APERTURE

One of the main problems of the previous lattice was the small dynamic aperture - in the horizontal plane 10 σ_x maximum, corresponding to 20. mm, - which was still reduced for the off-energy particles. In particular, due to the high chromaticity and the small β separation, together with the lack of good locations available for the sextupoles, the tunes behaviour with $\Delta p/p$ was badly corrected, and the maximum $\Delta p/p$, where a fairly good dynamic aperture was achievable, was .5%. Attempts to correct the harmonic behaviour of the lattice with a specific code (CATS)[2], didn't lead to improvements.

The new lattice presented here has three main features:

- The better separation of the optical functions in the arcs allows a more efficient chromaticity correction, with lower sextupole strengths and therefore less sensitivity to the resonances and a better dynamic aperture.

- The total tunes, 4.87 for the horizontal and 4.85 for the vertical one, are quite far from the integer. The tune diagram is shown in **Fig. 4.1.** The resulting tune dependence from the energy is very much improved, as shown in **Fig. 4.2**, so that the dynamic aperture doesn't change very much also for particles with a momentum deviation of 1%, a very good result for the Touscheck lifetime. The beta functions behaviour with energy, shown in **Fig. 4.3**, is good too.

- The tracking performed, with the code PATRICIA[3], for several tune values has shown that the best results are obtained when, keeping constant the total tunes, the vertical tunes of the *Short* and *Long* are quite far away one from the other, that is when $\nu_y^{(short)}$ is larger than $\nu_y^{(long)}$, since the phase advance between the sextupoles is more favourable. The best dynamic aperture was obtained for lattices with a tune difference $\Delta\nu_y$ of .39, but also for a $\Delta\nu_y$ of .33, as in the chosen lattice, there is a substantial improvement.

The best sextupole configuration, presented in **Table 4.I**, - where the SF's have negative strengths and SD's have positive ones - consists of six families (12 multipoles per ring) - four in the achromats of the *Short* and *Long*, and the last two respectively one before the first bending of the *Long* and the other in the injection section. In Table 4.I the last column lists the sextupole gradient values at 510 MeV assuming .2 m long sextupole. They give a very good tunes behaviour as a function of the particle amplitude, see **Figs. 4.4** and **4.5**, even if there are no sextupoles in the dispersion free region.

Table 4.I

	SEXT. NAME	BETAX(M)	BETAY(M)	MUX	MUY	DX(M)	Ks (m-2)	B"(T/m2)
I.P.1								
	SDL4	10.24	8.06	0.24	0.39	-0.61	0.30	2.60
	SDL3	0.70	4.22	0.40	0.45	1.38	4.60	39.10
	SFL2	10.63	1.31	0.72	0.87	1.97	-2.00	17.00
	SDL1	2.68	8.87	0.79	0.99	0.43	1.00	8.50
SYML								
	SDL1	2.68	8.87	1.89	1.27	0.43	1.00	8.50
	SFL2	10.63	1.31	1.96	1.39	1.97	-2.00	17.00
	SDL3	0.70	4.22	2.28	1.81	1.38	4.60	39.10
	SDL4	10.24	8.06	2.45	1.87	-0.61	0.30	2.60
I.P.2								
	SDS2	0.81	4.10	3.15	2.71	1.68	12.65	107.50
	SFS1	7.91	1.31	3.39	3.12	1.07	-3.40	28.90
SYMS								
	SFS1	7.91	1.31	4.16	3.99	1.07	-3.40	28.90
	SDS2	0.81	4.10	4.40	4.41	1.68	12.65	107.50

The resulting dynamic aperture, 16 σ_x maximum - corresponding to 34 mm in the horizontal plane - is very good in the vertical plane too, as shown in **Fig. 4.6**, where the L-1 dynamic aperture is plotted for comparison.

Fig. 4.7 shows the results for the off-energy particles, compared to the unperturbed ones. The situation remains mainly unchanged: a small reduction for positive energy deviations and an increase for the negative ones. For comparison the physical aperture is shown on the same scale. In **Figs. 4.8** and **4.9** the off energy dynamic apertures (for $\Delta P/P$ = .7%) are compared to the L-1 ones. It has to be noted that the previous structure was unstable for values of $\Delta P/P$ larger than .7%. In **Fig. 4.10** is plotted the dynamic aperture as computed by CATS, at the symmetry point of the *Long*, compared to the stability boundaries due to the main third order resonances. It is clear from this picture that no low-order resonance is limiting the dynamic aperture.

In conclusion, we think that the new lattice seems to have all the characteristics to assure a good dynamic aperture, together with a good beam lifetime.

5. MULTIPOLE ERRORS SENSITIVITY

The effect of multipole errors in the magnetic elements on the dynamic aperture has been simulated with the code Patricia. We have considered separately the effect of each type of error. The vertical field is written as:

$$B_z = B_0\, \rho \sum_{i=0}^{n} k_n \frac{x^n}{n!} \ .$$

From this formula we get the strength for the multipolar coefficients k_n, assuming for each one a value of $\Delta B/B = 5\ 10^{-4}$ at 3 cm from the center. We have considered dodecapoles in the quadrupoles and sextupoles and decapoles in the dipoles, no multipoles have been added in the low-β quadrupoles which have been treated separately below. The used multipolar coefficients are listed in **Table 5.I**. For each multipole component it has been computed the dynamic aperture for three different values of the relative energy deviation ($\Delta p/p$ = +1%,0 and -1%) and for the positive and negative sign of the multipole component. In **Figs. 5.1** to **5.6**, the obtained dynamic apertures for the three energies are shown on the same plot with the reference dynamic aperture for the ideal machine.

Table 5.I

		Dipoles	Q-poles
sextupole	**k_2** (m^{-3})	.7937	—
decapole	**k_4** (m^{-5})	10.582	—
dodecapole	**k_5 / k_1** (m^{-4})	—	74074.

It has to be noted that the quadrupole design is not very demanding, because the strengths are quite small, while the design of the bending magnets is more difficult because of the small bending radius, in fact the multipolar components in the dipoles depend on the inverse of the bending radius.

Dodecapoles in the quadrupoles (**Figs. 5.1a,b,c**)**:** the dodecapole component has nearly no effect on the dynamic aperture for zero and positive $\Delta p/p$, while gives a strong reduction for the negative $\Delta p/p$. Anyway this is not dramatic, first of all because 1% is a very large energy deviation, near the limit of the required acceptance and we do not need all the transverse aperture. Besides, the value of the dodecapole component computed by the magnet design code [4] is well below the value we have assumed for these simulations.

Sextupoles in the dipoles (**Figs. 5.2a,b,c**)**:** the sextupoles in dipoles have been inserted as isolated multipoles in order to keep constant the chromaticity correcting sextupoles SF and SD. Their presence does not give a sensible reduction of the dynamic aperture except for negative energy. For all the energies the negative sextupolar component (negative sextupoles correct the horizontal chromaticity) gives a larger dynamic aperture than the positive one.

Decapoles in the dipoles (**Figs. 5.3a,b,c**)**:** in this case there is a sensible reduction also for zero energy deviation, and a quite strong reduction for the negative energy. Therefore the decapole contents of the dipole field has to be lower than the value used in this simulation.

Dodecapoles in the low-β quadrupoles (**Figs. 5.4a,b,c**)**:** these quadrupoles are different from the others because the beam passes through them off-axis, moreover the design is different because, in order to get a very small size, they will be permanent magnets. Due to the displacement of the trajectory with respect to the quadrupole center, a multipolar component with respect to the center(x=0) produces all the lower order components respect to a displaced position x_0. In **Table 5.II** for the three quadrupoles the multipole components corresponding to a dodecapole of $\Delta B/B=5\times10^{-4}$ at 3 cm are given. In this case there is a reduction of the dynamic aperture already for $\Delta p/p = 0$, therefore it is important to reduce the intensity of the dodecapole component in the quadrupole design. A prototype has been done for this quadrupoles and magnetic measurements are in progress. As soon as the measurements will be completed a more realistic simulation will be done using the measured values of the multipoles. As the dynamic aperture for the negative $\Delta p/p$ (-1%) is very small, it has been computed also for $\Delta p/p$ =-.5% and the result is $\sim 10\sigma_x$ in the horizontal plane, which is quite satisfactory (see **Fig. 5.5**).

Table 5.II

Dodecapoles in low-β quads

		Q1	**Q2**	**Q3**
Δ**x** (mm) - quad center		5.316	8.427	18.426
dodecapole	k_5 (m^{-6})	3.22×10^5	5.18×10^5	2.93×10^5
decapole	k_4 (m^{-5})	1711.75	4369.41	5391.43
octupole	k_3 (m^{-4})	4.55	18.41	49.67
sextupole	k_2 (m^{-3})	.008	.052	.305
quadrupole	k_1 (m^{-2})	1.07×10^{-5}	10.9×10^{-5}	140.5×10^{-5}
dipole	k_0 (m^{-1})	1.14×10^{-8}	1.84×10^{-7}	5.17×10^{-6}

Sextupoles in the wigglers (**Figs. 5.6a,b,c**)**:** thin lens sextupoles have been inserted at both edges of each pole and half-pole, with alternate signs. The integrated strength S_2 is obtained from the sextupolar coefficient k_2 at the pole center taking into account the sinusoidal behaviour of the field:

$$S_2\,[\mathrm{m}^{-2}] = \frac{k_2\, l_p}{2\pi},\quad l_p = \text{period length.}$$

The used strengths of the sextupole component in the wiggler:

$$S_2 = 2.89\ \mathrm{m}^{-2} \qquad \text{for each pole,}$$

and

$$S_2 = 1.44\ \mathrm{m}^{-2} \qquad \text{for each half-pole,}$$

were computed using a calculated value[4] of the sestupolar coefficient in the field expansion. Although the strength is quite high and of the same order of magnitude of the sextupoles used to correct the chromaticity, the effect on the dynamic aperture is completely negligible.

It has to be noted that for all the examples shown above the negative $\Delta p/p$ case is always worse than the other two. The reason for this might be the fact that the betatron tunes as a function of the energy (see Fig.4.2) cross each other for $\Delta p/p \approx -.9\%$, therefore the dynamic aperture should be calculated for smaller values of $\Delta p/p$. Anyway before going on with further simulations it is better to wait for an estimate of the multipole terms present in the real magnets.

6. ALIGNMENT TOLERANCES AND ORBIT CORRECTION

In this chapter we report the results of our investigation on closed orbit distortions due to misalignments and field errors in magnets. As already discussed in a previous note (L-3)[5], the idea is to run the machine without sextupoles at the start-up, operating at low current, to look for the closed orbit and to perform a first alignment correction. At this stage the possibility of a quadrupole mechanical displacement, to correct the orbit distortion, is foreseen. Later on one can operate the machine with all the sextupoles on and use the appropriate corrector scheme to minimize the residual closed orbit distortion.

The computer code MAD[6] has been used to study the machine sensitivity to errors and to look for an optimal corrector configuration. The code generates random error distributions with a given standard deviation in order to assign alignment, field and rotation errors to the magnetic elements. After that it calculates the closed orbit through all the lattice (each error distribution corresponds to a different machine configuration).

In order to study the lattice sensitivity to errors we have assigned transverse disalignments (Δx,Δy), rotations around the transverse axes ($\Delta\theta$, $\Delta\Phi$) and magnetic field errors ($\Delta B/B$) to bendings and quadrupoles separately. Two values have been considered for each type of error, simulating 5 machines per case. No sextupoles are included in the lattice at this stage. The error values assumed come from experience in operating machines:

$$\Delta x = \Delta y = 0.1 \text{ mm and } 0.2 \text{ mm}$$

$$\Delta\theta = \Delta\Phi = 0.175 \text{ mrad and } 0.25 \text{ mrad}$$

$$\Delta B/B = 5 \times 10^{-4} \text{ and } 8 \times 10^{-4}$$

The Tables where the results are summarized contain all the parameters of interest that can be strongly affected by these imperfections, like β-function at IP and dispersion.

In **Table 6.I/a** the average and maximum values for the closed orbit amplitude in both transverse planes are reported. The Table shows that the closed orbit is quite sensitive to field errors in bendings (see x-plane) and to quadrupole displacements. In any case the particle orbit remains inside the physical aperture of the machine, ± 4 cm in horizontal and ± 3 cm in vertical (the case with $\Delta B/B$ equal to $8\text{x}10^{-4}$ is rather extreme).

Because the new lattice is not much different from the previous one, in this analysis we used a monitor distribution similar to the one described in L-3; some positions have been changed due to the different locations of β-function maxima in both planes (see **Fig. 6.1** for one quart of the machine). There are 20 beam position monitors acting in both planes plus 6 only horizontal and 4 only vertical.

No errors have been included in the wigglers, that are to be considered as a separate problem.

To get an idea of the needed correction in the interaction region, errors (displacements and tilts) have been simulated also in the low-β quads.

Table 6.I/b shows the results: these errors roughly double the closed orbit amplitude in both planes, still leaving the orbit inside the geometrical aperture of the machine. The data show that we can accept displacement errors of ±0.2 mm. However, in the following no imperfections have been put in these quadrupoles, considering, at the first stage, the possibility of correcting the orbit by just moving the magnetic elements, and that in this region there is lack of space for correctors and monitors.

Table 6.II shows the values of some machine parameters obtained by averaging the data from 10 simulated machines.

TABLE 6.I/a

Closed orbit distortion due to single types of errors

(low-β quads without errors)

Type of error		in quadrupoles	in bending magnets
$\Delta x, \Delta y$ =.1 mm	X_{rms} (mm)	1.5±.7	.34±.22
	X_{max} (mm)	3.4±1.5	.81±.51
	Y_{rms} (mm)	1.5±1.0	.27±.17
	Y_{max} (mm)	4.3±2.6	.65±.36
$\Delta x, \Delta y$ =.2 mm	X_{rms} (mm)	3.0±1.4	.68±.44
	X_{max} (mm)	6.7±3.0	1.6±1.0
	Y_{rms} (mm)	3.0±2.1	.54±.35
	Y_{max} (mm)	8.5±5.2	1.3±.7
$\Delta\Theta, \Delta\Phi$ =.175 mrad	X_{rms} (mm)	.42±.23	.41±.20
	X_{max} (mm)	.86±.39	.85±.44
	Y_{rms} (mm)	.36±.19	.49±.13
	Y_{max} (mm)	1.08±.45	1.13±.28
$\Delta\Theta, \Delta\Phi$ =.25 mrad	X_{rms} (mm)	.59±.33	.59±.29
	X_{max} (mm)	1.23±.56	1.21±.63
	Y_{rms} (mm)	.51±.28	.70±.19
	Y_{max} (mm)	1.55±.64	1.6±.41
$\Delta B/B$ = 5×10^{-4}	X_{rms} (mm)		8.1±4.4
	X_{max} (mm)		18.06±9.13
$\Delta B/B$ = 8×10^{-4}	X_{rms} (mm)		13.0±6.9
	X_{max} (mm)		28.8±14.3

TABLE 6.I/b

including low-β quadrupoles with errors

Type of error		in quadrupoles
$\Delta x, \Delta y$ =.1 mm	X_{rms} (mm)	2.86±1.09
	X_{max} (mm)	6.73±2.46
	Y_{rms} (mm)	3.40±1.24
	Y_{max} (mm)	8.53±2.27
$\Delta\Theta, \Delta\Phi$ =.175 mrad	X_{rms} (mm)	0.47±0.36
	X_{max} (mm)	1.08±0.74
	Y_{rms} (mm)	.74±.45
	Y_{max} (mm)	2.01±1.27

TABLE 6.II

Closed orbit parameters before and after correction
Monitors: 20 HV, 6H, 4V -- Correctors: 18H, 16V (sextupoles off)
Δx=Δy =.2mm, $\Delta\Theta$=$\Delta\Phi$ =.25 mrad, $\Delta B/B$ = 5x10^{-4}

	ideal machine	before correction	after correction
X_{rms}(mm)	0	8.9±6.4	0.34±0.13
X_{max}(mm)	0	18.4±10.9	1.1± 0.4
Y_{rms}(mm)	0	3.5±1.8	0.24±0.06
Y_{max}(mm)	0	9.53±5.01	0.71±0.13
η_{Xrms}(m)	1.17	1.31±.16	1.1714±.0004
η_{Xmax}(m)	2.16	2.72±.41	2.1603±.0023
η_{Yrms}(m)	0	.41±.26	0.005±.002
η_{Ymax}(m)	0	1.07±.70	0.013±.006
α_{Xrms}(mrad)	0		0.46±0.10
α_{Xmax}(mrad)	0		1.05±0.27
α_{Yrms}(mrad)	0		0.23±0.07
α_{Ymax}(mrad)	0		0.64±0.28
Q_X	4.87	4.8704±0.0015	4.8705±0.0007
Q_y	4.85	4.852±0.003	4.8504±0.0009
β_X (m) @ IP	4.5	4.51±0.04	4.49±0.03
β_y (m) @ IP	0.045	0.0455±0.0017	0.0452±0.0004
η_X(m) @ IP	0	0.06±0.53	.002±0.004
η_Y(m) @ IP	0	0.006±0.034	.0001±0.0003

We assumed the following errors:

$$\Delta x = \Delta y = 0.2 \text{ mm}$$

$$\Delta\theta = \Delta\Phi = 0.25 \text{ mrad}$$

$$\Delta B/B= 5 \times 10^{-4}$$

in all bends and quads excluding low-β ones, with sextupoles off. We maintain the same monitor configuration as before adding correctors in position dictated by high β locations and available space in the lattice. The proposed layout, see Fig. 6.1, includes 18 correctors acting in horizontal plane and 16 in vertical one.

In the Table the data before and after the correction are reported, compared with the ideal ones. The results are really good, leaving a residual maximum amplitude of 1.1 mm in the horizontal plane and .71 mm in the vertical with a maximum corrector strength of 1 mrad.

The same work including the sextupoles and adding errors also in them has been carried out. **Table 6.III** shows the results obtained averaging over 10 machines (note that we ran 12 machines, but 2 were unstables). The data after the correction are about the same as before, showing only an higher vertical residual dispersion. It has to be mentioned that the residual dispersion at IP is really negligible. **Figs. 6.2** and **6.3** show the plots of the closed orbit amplitude as measured at monitor locations before and after correction for horizontal and vertical plane respectively, for one simulated machine.

TABLE 6.III

Closed orbit parameters before and after correction
Monitors: 20 HV, 6H, 4V -- Correctors: 18H, 16V (sextupoles on)
$\Delta x = \Delta y = .2$mm, $\Delta\Theta = \Delta\Phi = .25$ mrad, $\Delta B/B = 5\text{x}10^{-4}$

	ideal machine	before correction	after correction
X_{rms}(mm)	0	7.7±5.7	0.36±0.11
X_{max}(mm)	0	16.8±10.9	1.11± 0.28
Y_{rms}(mm)	0	3.2±1.3	0.29±0.13
Y_{max}(mm)	0	8.48±3.38	0.83±0.35
η_{Xrms}(m)	1.17	1.31±.39	1.171±.005
η_{Xmax}(m)	2.16	2.52±.89	2.17±.02
η_{Yrms}(m)	0	.32±.24	0.032±.015
η_{Ymax}(m)	0	.84±.49	0.08±.04
α_{Xrms}(mrad)	0		0.46±0.10
α_{Xmax}(mrad)	0		1.01±0.25
α_{Yrms}(mrad)	0		0.23±0.07
α_{Ymax}(mrad)	0		0.66±0.28
Q_X	4.87	4.871±0.022	4.8704±0.0014
Q_Y	4.85	4.859±0.038	4.849±0.002
β_X (m) @ IP	4.5	4.49±0.58	4.52±0.02
β_Y (m) @ IP	0.045	0.0456±0.012	0.0450±.0005
η_X(m) @ IP	0	-.18±0.30	-.007±0.031
η_Y(m) @ IP	0	-0.009±0.038	-.0009±0.0028
$Y_{c.o.}$ (mm)@ IP	0	-.12±.32	-0.007±0.008

For the same testing machine we report the plots of the closed orbit, before and after correction, along the whole structure in **Figs. 6.4** and **6.5** for horizontal and vertical plane respectively; the graphics start at one IP going before trough the *Short* lattice and then in the *Long*. The sample case used respects the medium behaviour of the orbit.

Finally we have considered monitor alignment errors (±0.1 mm and ±0.2 mm) in both transverse planes. **Table 6.IV** shows the averaged data before and after correction using 10 machines for both error values. The results are satisfactory showing a maximum residual orbit less than 1.5 mm in the horizontal plane and around 1 mm in the vertical one. The required corrector strength is always under 1 mrad. The horizontal dispersion @ IP is roughly 1 cm.

TABLE 6.IV

Closed orbit parameters before and after correction
Monitors: 20 HV, 6H, 4V -- Correctors: 18H, 16V (sextupoles on)
$\Delta x=\Delta y$ =.2mm, $\Delta\Theta=\Delta\Phi$ =.25 mrad, $\Delta B/B = 5x10^{-4}$

Errors in monitors, $\Delta x=\Delta y$

	ideal machine	before cor.	after correction $\Delta x=\Delta y$=.1 mm	after correction $\Delta x=\Delta y$=.2 mm
X_{rms}(mm)	0	7.7±5.7	0.38±0.13	0.44±0.16
X_{max}(mm)	0	16.8±10.9	1.24± 0.35	1.35±0.48
Y_{rms}(mm)	0	3.2±1.3	0.31±0.11	0.36±0.09
Y_{max}(mm)	0	8.48±3.38	0.90±0.28	1.01±0.25
η_{Xrms}(m)	1.17	1.31±.39	1.171±.004	1.171±.005
η_{Xmax}(m)	2.16	2.52±.89	2.17±.02	2.17±.02
η_{Yrms}(m)	0	.32±.24	0.03±.01	0.032±.016
η_{Ymax}(m)	0	.84±.49	0.08±.039	0.078±.039
α_{Xrms}(mrad)	0		0.45±0.08	0.46±0.09
α_{Xmax}(mrad)	0		0.98±0.17	0.96±0.23
α_{Yrms}(mrad)	0		0.26±0.08	0.31±0.09
α_{Ymax}(mrad)	0		0.67±0.30	0.72±0.29
Q_X	4.87	4.871±0.022	4.8701±0.0016	4.869±0.002
Q_y	4.85	4.859±0.038	4.849±0.002	4.849±0.003
β_X (m) @ IP	4.5	4.49±0.58	4.52±0.04	4.52.±.006
β_y (m) @ IP	0.045	0.0456±0.012	0.0451±.0008	0.0451±.0008
η_X(m) @ IP	0	-.18±0.30	-.011±0.037	-.014±0.046
η_Y(m) @ IP	0	-0.009±0.038	-.0008±.0027	-.0006±0.003

From the performed analysis we can conclude that, with the chosen error values, the orbit is always inside the physical aperture and that the correction can be done by "moving" quads in both transverse planes at first approximation. The presence of correctors assure an optimization of the correction and the control of the beam orbit during the runs. It has to be mentioned that a good correction has been obtained using correctors with a maximum strength of roughly 1 mrad.

7. BEAM LIFETIME AND VACUUM CHAMBER APERTURE

Due to the low energy of the machine, the main effect limiting the beam lifetime is the single Touschek scattering, which gives a lifetime proportional to the third power of the energy. The momentum deviation produced in the Coulomb scattering of the particles within the bunch depends on the bunch density and the rms angular divergence σ'_x. The Touschek lifetime has been calculated using the formulae in (ref.Bruck)[7], assuming that the machine acceptance is limited by the RF bucket height and by the transverse aperture (physical or dynamic aperture). To obtain the energy acceptance due to the transverse aperture, for each point s_i, it is calculated the quantity:

$$H(s_i) = \gamma(s_i)D_x^2(s_i) + 2\alpha(s_i)D_x(s_i)D_x'(s_i) + \beta(s_i)D_x'^2(s_i)$$

then the maximum oscillation all over the ring for a particle which has lost an energy Δp in s_i is:

$$x_{max}(s_i) = \max \left\{ \frac{\Delta p}{p} \left[\sqrt{H(s_i)\beta(s)} + \left| D_x(s) \right| \right] \right\}$$

The maximum energy acceptance for each point s_i isobtained for $x_{max} = R_x$:

$$\frac{\Delta p}{p}(s_i) = \frac{R_x}{\max \left[\sqrt{H(s_i)\beta(s)} + \left| D_x(s) \right| \right]}$$

where R_x is the vacuum chamber half-aperture.

To see which is the limiting factor, RF acceptance or physical aperture, we have plotted in **Figs. 7.1 and 7.2** the Touschek and total beam lifetimes as a function of the transverse aperture R_x and of the RF voltage V_{RF} respectively. The other parameters are set at the values given in **Table 7.I**, which correspond to the design values for the maximum luminosity.

Table 7.I

V_{RF} (KV)	254.5
RF acceptance ε_{RF}	1.23%
N part./bunch	8.9 10^{10}
<I> /bunch (mA)	43.75
Z/n (Ω)	2
bunch length σ_z (cm)	3
rel. energy spread	1.46 10^{-3}
coupling factor κ	.01
R_y (cm)	3
R_x (cm)	4

With these values we are in the anomalous lengthening regime and the bunch length has been calculated assuming a vacuum chamber broad band impedance of 2 Ω.

An R_x value of 2.5 cm, corresponding to ~$7\sigma_x$, gives already a good quantum lifetime, but from Fig.7.1 one can see that it is convenient to choose a larger aperture and that up to 10cm the beam lifetime is still increasing with the horizontal aperture.

The choice of the aperture is crucial for this machine because we want a high emittance (for high peak luminosity) and good beam lifetime (for average luminosity). Therefore we want the largest vacuum chamber aperture compatible with the technical constraints; moreover also the dynamic aperture has to be as large as the physical aperture.

The most critical elements are the low-β quadrupoles, which have a strict limitation on the outer dimension, the bending magnets which need a very good field quality on the transverse aperture and the wiggler magnets, where to the required aperture has to be added the excursion of the reference trajectory.

We have chosen a value of R_x=4 cm, which is compatible with the technical constraints in the design of the magnetic elements and is as large as the dynamic aperture. This gives a Touschek beam lifetime of nearly three hours.

With this value of the aperture the dependence of the Touschek lifetime on the RF voltage is shown in Fig. 7.2. The lifetime is growing very fast up to 100 KV, which correspond to a bucket height of $6\sigma_p$ (the minimum required for quantum lifetime), then has a maximum around the design voltage and decreases slightly for higher voltages. This behaviour is more clear looking at the dependence of the lifetime on the RF acceptance, for a fixed bunch length, shown in **Fig. 7.3**.

The Touschek beam lifetime increases with the RF acceptance up to a value where the limit is due only to the vacuum chamber aperture and then saturates. Varying the RF voltage the energy acceptance increases with the square root of it, but the bunch length gets smaller, giving a higher bunch density. When the limitation is entirely due to the aperture a further increase of the RF voltage gives a reduction of the lifetime with the bunch length.

The above calculations have been done for the extreme values of the design parameters, in particular the highest bunch current and the minimum coupling factor, which give the minimum Touschek beam lifetime expected. If we adopt a larger value of the coupling factor the beam lifetime increases as shown in **Table 7.II**.

Table 7.II

κ	$\tau_{TOUSCHEK}$ (min)	τ_{TOTAL} (min)
.01	207	156
.02	289	198
.10	597	307

The dependence of the Touschek and total beam lifetime as a function of the average beam current in the bunch is shown in **Fig. 7.4**.

The vertical vacuum chamber aperture has been chosen in order to get a good value of the gas scattering beam lifetime τ_{SC}. The lifetime as a function of the vertical half-aperture R_y, assuming a gas pressure of 1nTorr with a nitrogen equivalent gas composition (Z = 8), is shown in **Fig. 7.5.** The two curves correspond to an horizontal aperture of 4 cm and 1m (practically infinite) respectively, in the last case τ_{SC} is simply proportional to the square of the aperture. R_y is the aperture at the maximum β_y location, in the second of the low-β quadrupoles, therefore we have chosen a value of 3 cm, which is the maximum feasible with the constraints on the outer dimensions given by the detector. With this value and 1nTorr pressure the scattering lifetime is ~17 hours, i.e. five times larger than the Touschek lifetime, and therefore has a small influence on the total lifetime.

In **Table 7.III** the contributions of the various phenomena to the beam lifetime for the single beam mode are listed, together with the beam-beam bremsstrahlung lifetime, for the parameter set of Table 7.I. Here we want to point out that, due to the choice of many bunches and high crossing frequency, the beam-beam bremsstrahlung gives a negligible contribution to the beam lifetime also at the maximum luminosity.

Table 7.III

BEAM PARAMETERS & dN/dt FOR T=293K - P=1nTorr - Z(biatomic)=8 :

REV. FREQUENCY (MHZ)	0.306880443D+01
HARMONIC NUMBER	0.120000000D+03
RF FREQUENCY (MHZ)	0.368256532D+03
VRF(KV)	0.254500000D+03
ENERGY (MEV)	0.510000000D+03
U0 (KeV)	0.930117996D+01
MOM. COMPACTION	0.166131298D-01
F SYNC.(KHz)	0.386019568D+02
RF ACCEPTANCE	0.122602203D-01
NAT.BUNCH LENGTH(cm)	0.814887835D+00
NAT. ENERGY SPREAD	0.396839470D-03
# ELECTRONS/BUNCH	0.889910504D+11
AV.CURRENT/BUNCH(mA)	0.437500000D+02
PEAK CURRENT/BUNCH(A)	0.209238587D+03
Z/n (Ohm)	0.200000000D+01
PEAK CURRENT M.W. Thres. (A)	0.419180653D+01
ANOMALOUS BUNCH LENGTHENING QUANTITIES :	
AN. BUNCH LENGTH(cm)	0.300039213D+01
REL. R.M.S. ENERGY-SPREAD	0.146115081D-02
PEAK CURRENT/BUNCH(A)	0.568278985D+02
EMITTANCE (mm-mrad)	0.100000373D+01
EMITTANCE COUPL.	0.100000000D-01
HOR. HALF-APERTURE (cm)	0.400000000D+01
VER. HALF-APERTURE (cm)	0.300000000D+01
QUANTUM LIFE (hrs)-SANDS	0.136398390D+09
LIFETIME GB (min)	2130.
LIFETIME SC (min)	1010.
LIFETIME GBe (min)	13103.
LIFETIME SCe (min)	22459.
TOUSCHEK (min)	207.
LIFETIME TOT.(min)	156.
TWO BEAMS LIFETIME @ L= 6.0e32 cm-2s-1	
LIFETIME BEAM-BEAM BREMS. (min)	1426.
LIFETIME TOT.(min)	141.

In **Fig. 7.6** the behaviour of the required aperture along half of the ring for R_x = 4 cm and R_y = 3 cm is shown. It corresponds to a beam size of 10 σ_x (off-coupling), 10 σ_p and 9 σ_y (full coupling).

As a conclusion we can say that the choice of the RF parameters is not critical for the Touschek lifetime while the aperture choice is determinant. A value of R_x = 4 cm seems to be a good compromise with the technical constraints and gives a total lifetime greater than 2 hours.

REFERENCES

[1] M. Bassetti, M.E. Biagini, C. Biscari, S. Guiducci, M.R. Masullo, G. Vignola: “High Emittance Lattice for DAΦNE”, DAΦNE Technical Note L-1, 30/10/1991.

[2] R. Nagaoka: “CATS”, Sincrotrone Trieste ST/M-91/3.

[3] H. Wiedemann: “Users guide for PATRICIA Version 85.5”, SSRL ACD Note 29.

[4] C. Sanelli, private communication.

[5] M.R. Masullo: “Orbit Correction Analysis for DAΦNE Lattice”, DAΦNE Technical Note L-3, 12/4/1991.

[6] H. Grote, F.C. Iselin: “The MAD Program”, CERN/SL/90-13 (AP).

[7] H. Bruck: “Accélérateurs circulaires de particules”, Presses Univérsitaires de France, 1966.

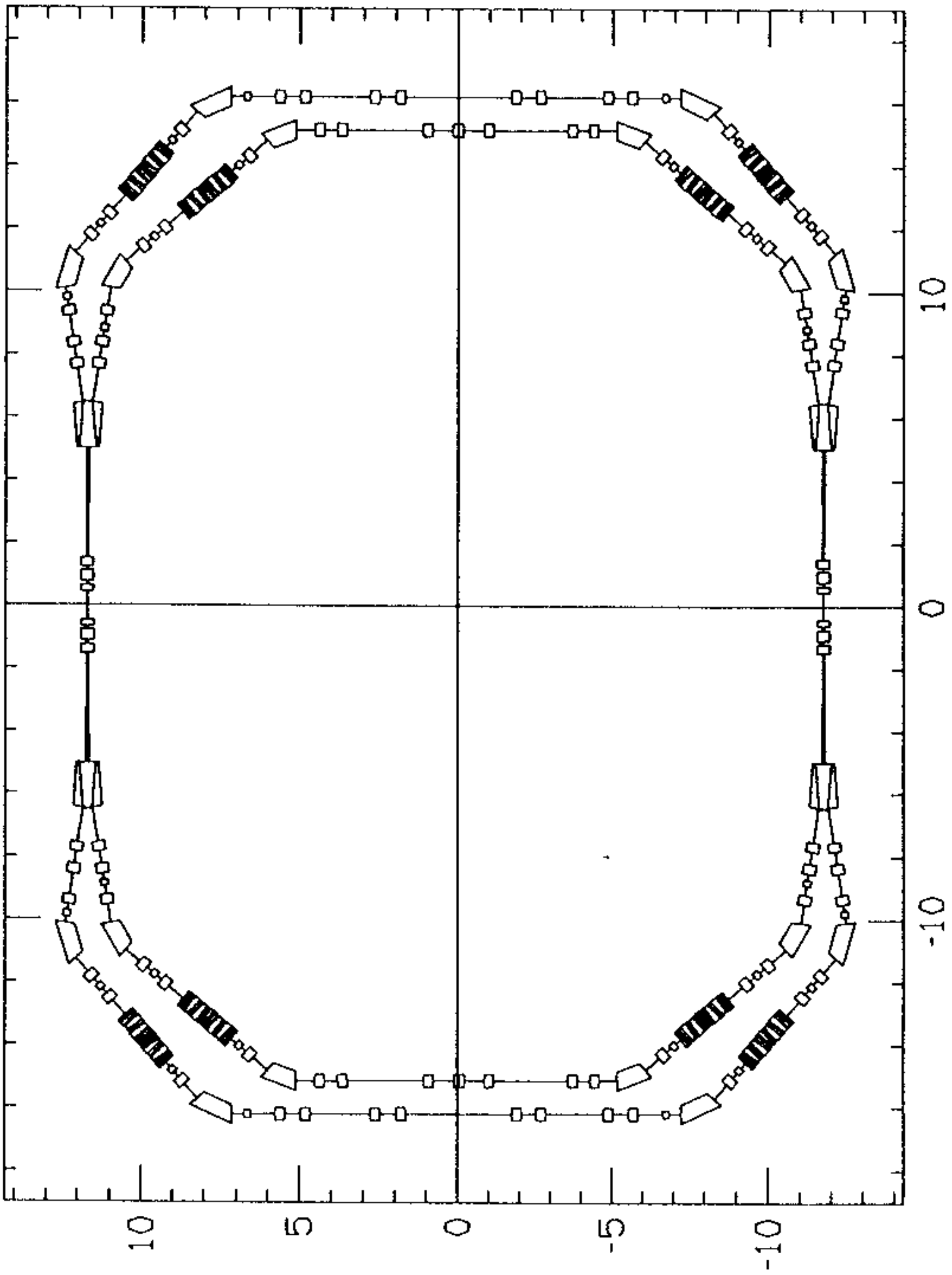

Fig. 2.1 - Layout of the DAΦNE storage rings.

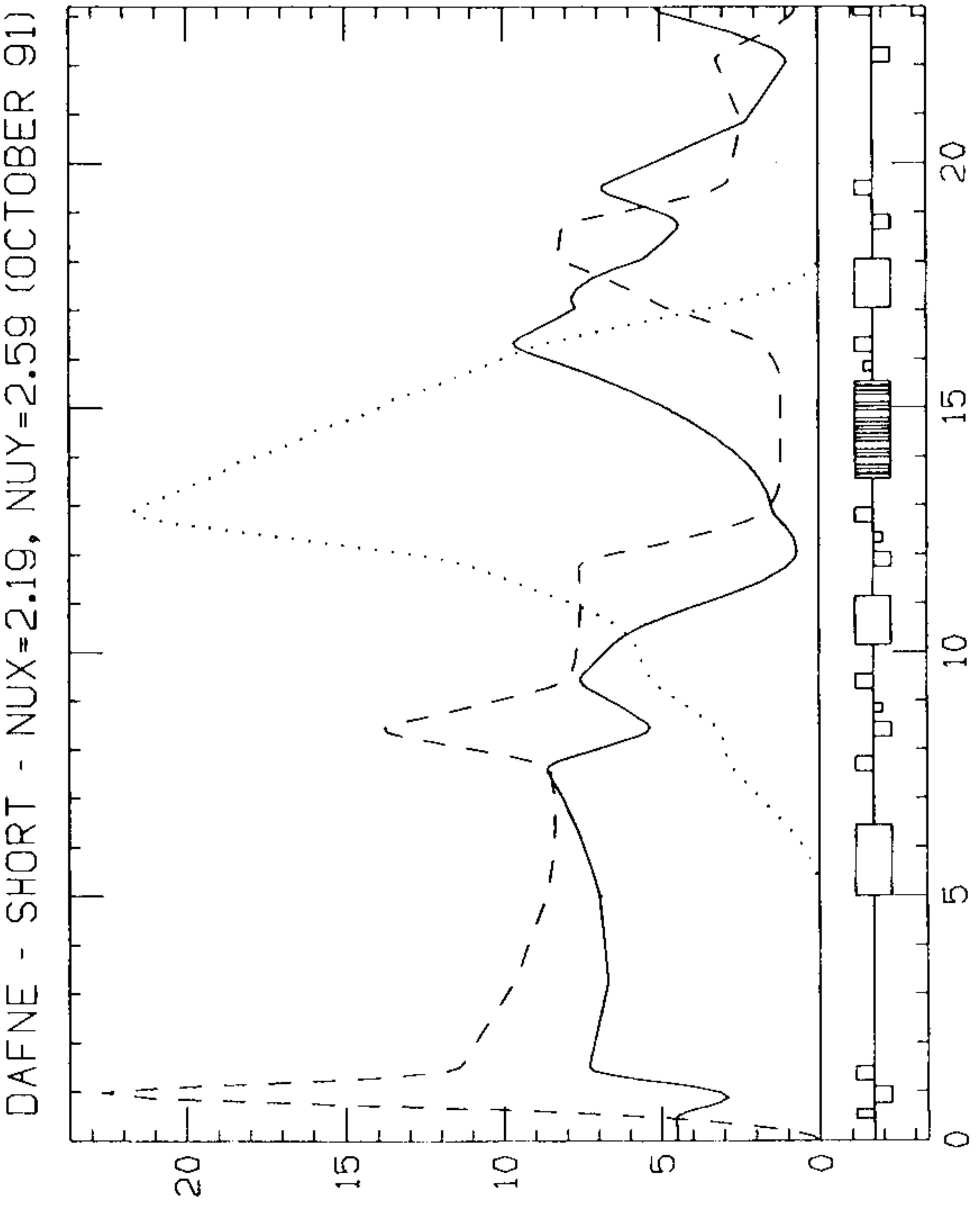

Fig. 3.1 - Optical functions for half of the *Short* section.

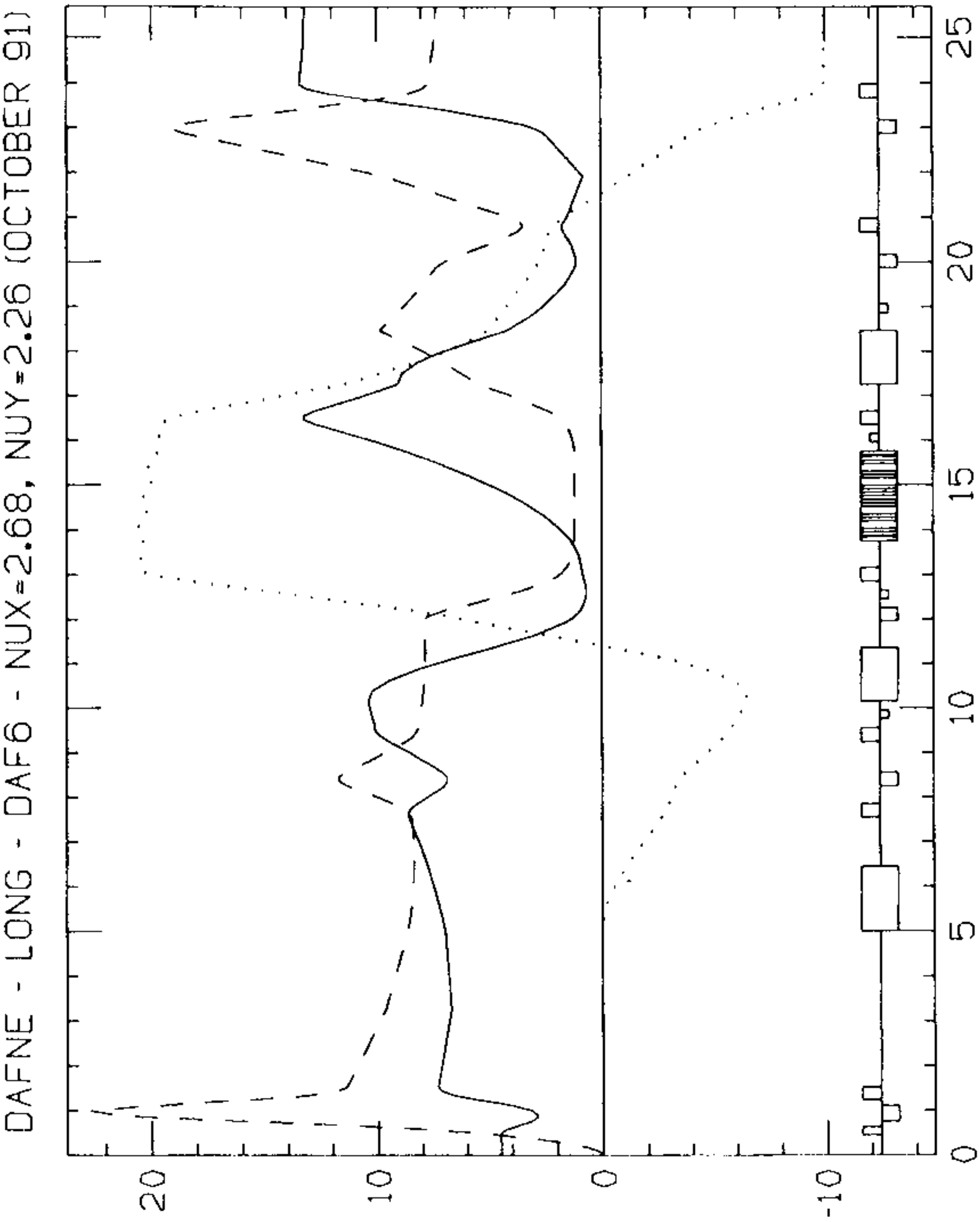

Fig. 3.2 - Optical functions for half of the *Long* section.

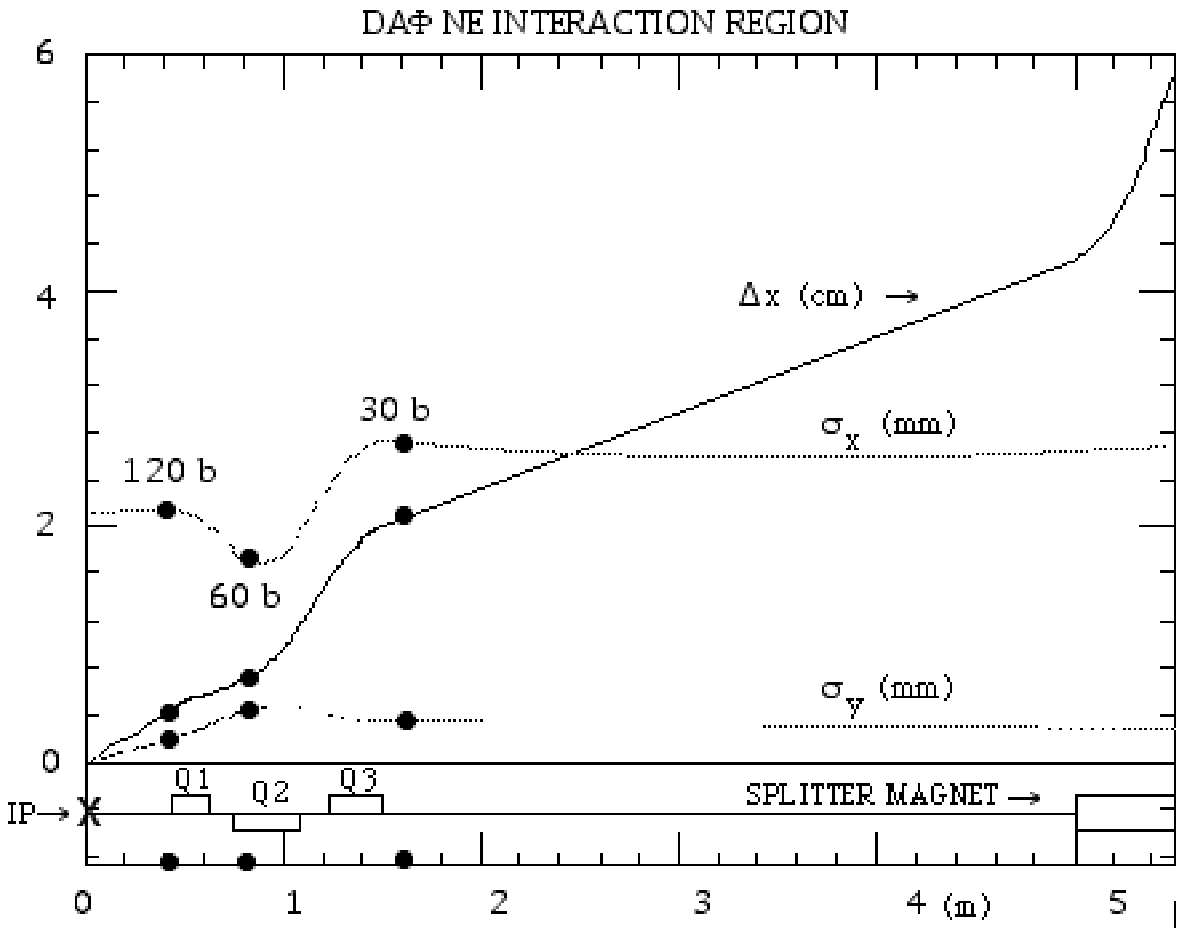

Fig. 3.3 - Half separation Δx between two beams and beam sizes σ_x, σ_y in the low-β insertion.

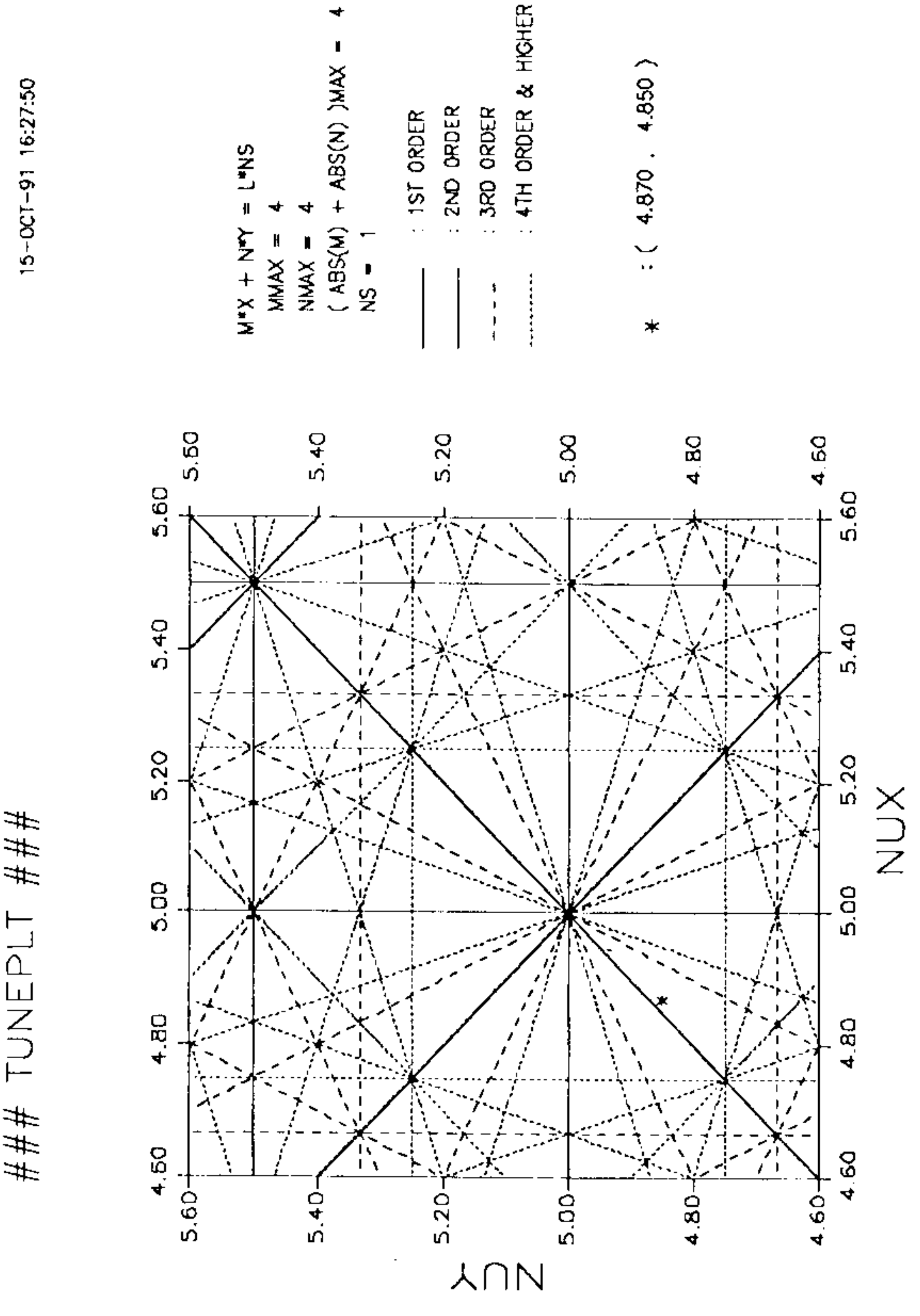

Fig. 4.1 - Tune diagram.

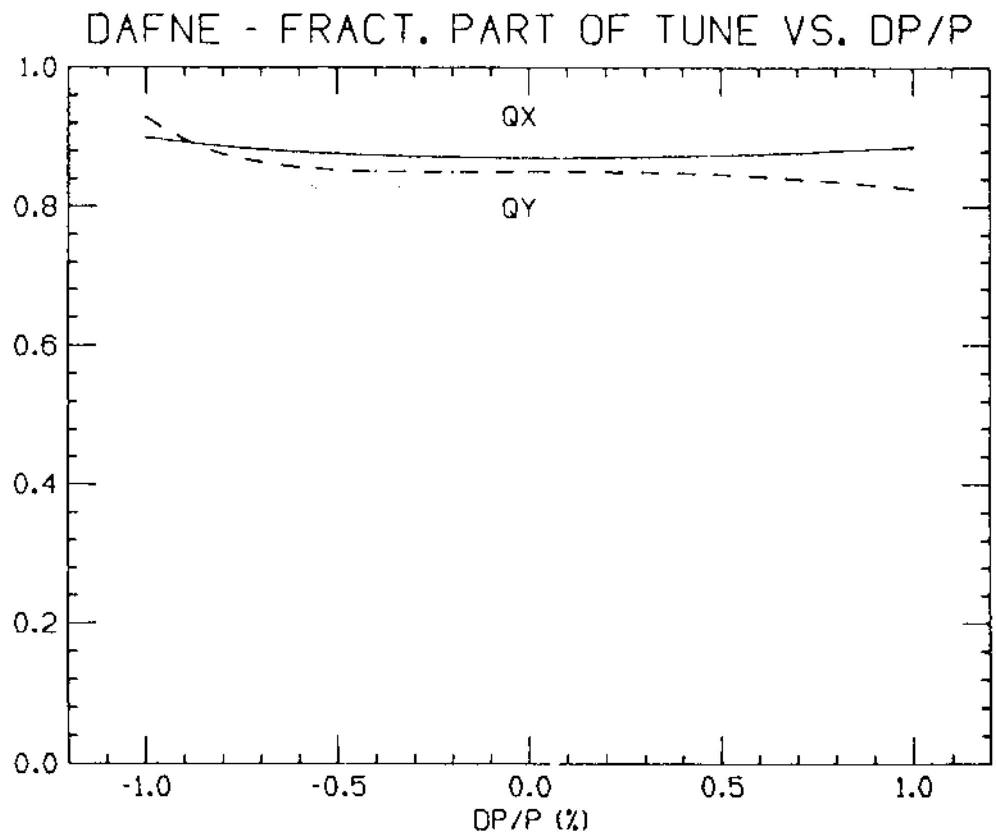

Fig. 4.2 - Betatron tunes versus relative energy deviation.

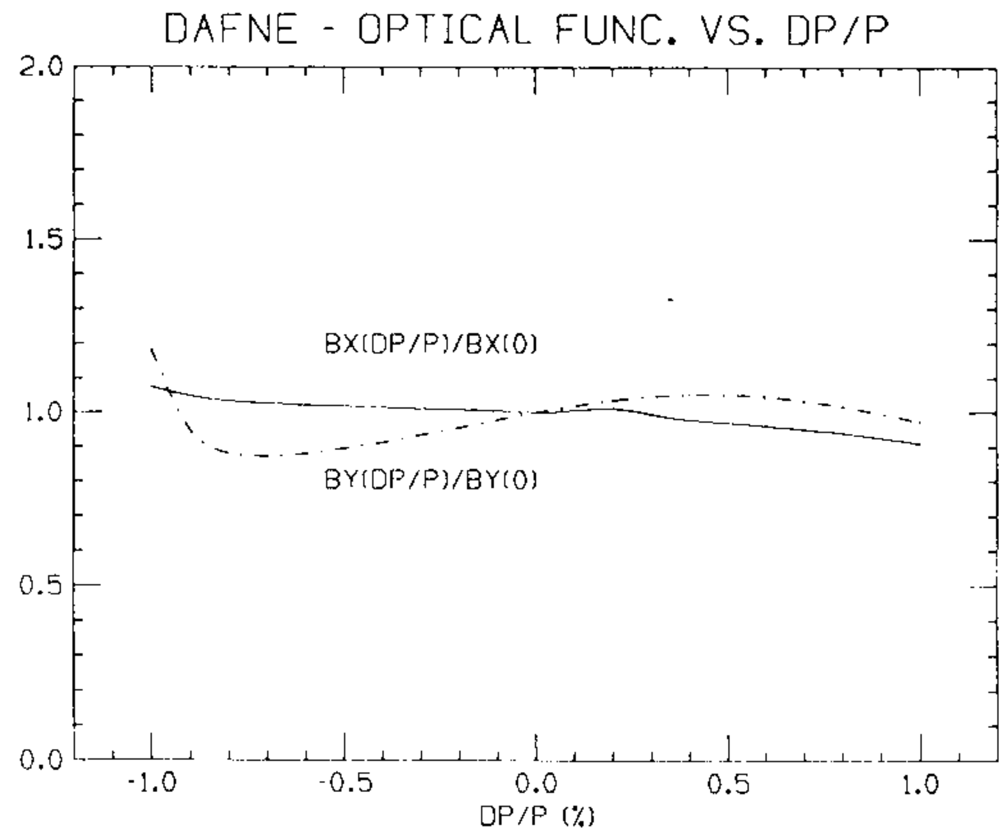

Fig. 4.3- β-functions versus relative energy deviation.

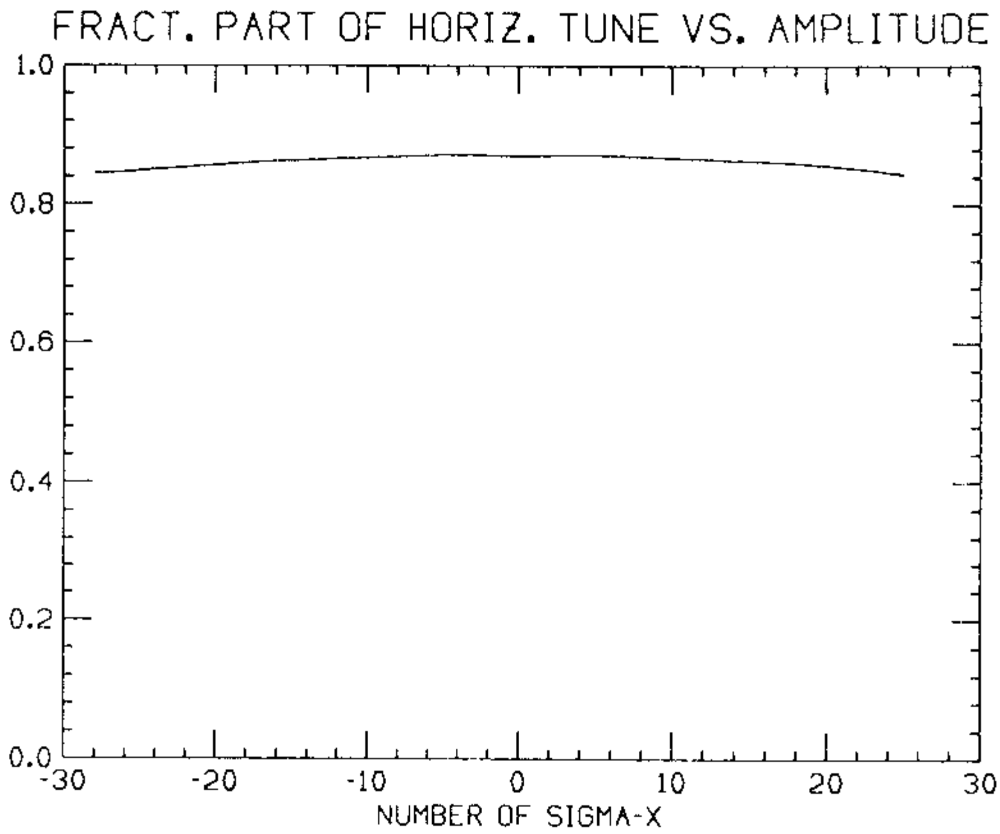

Fig. 4.4 - Horizontal betatron tune versus oscillation amplitude.

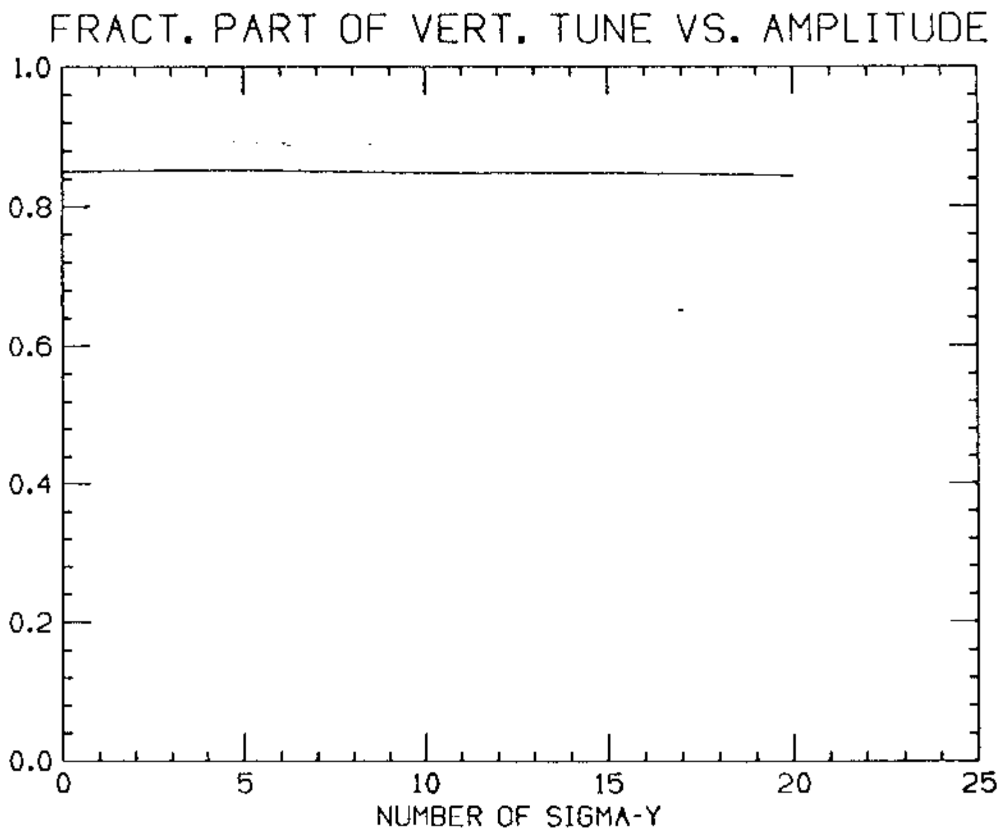

Fig. 4.5 - Vertical betatron tune versus oscillation amplitude.

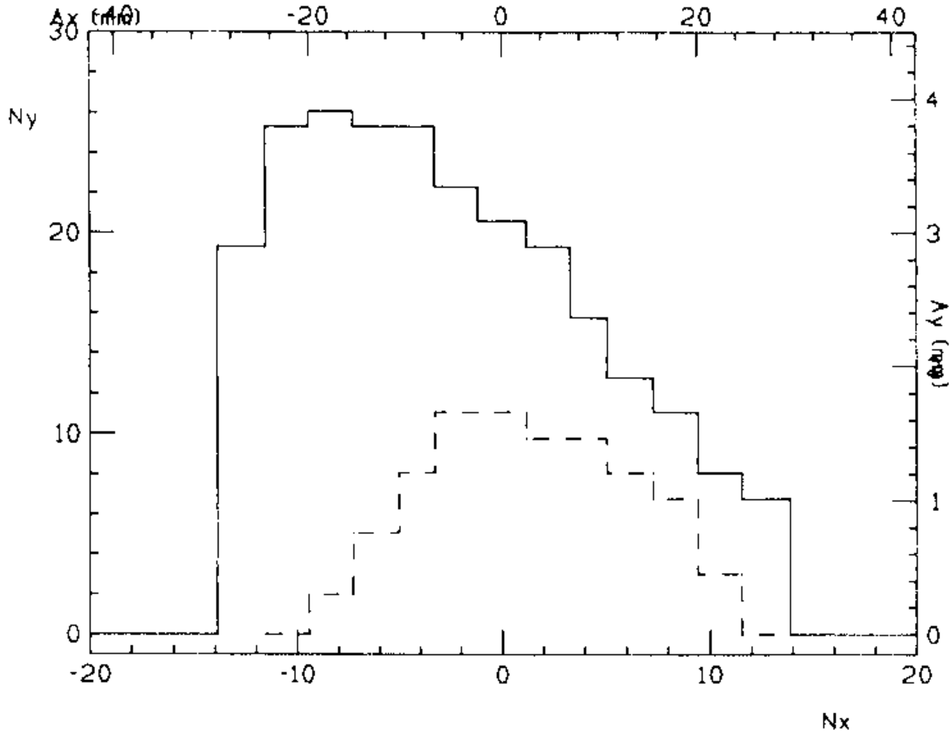

Fig. 4.6 - On energy dynamic aperture at I.P. (—) compared to the L-1 one (- - -).

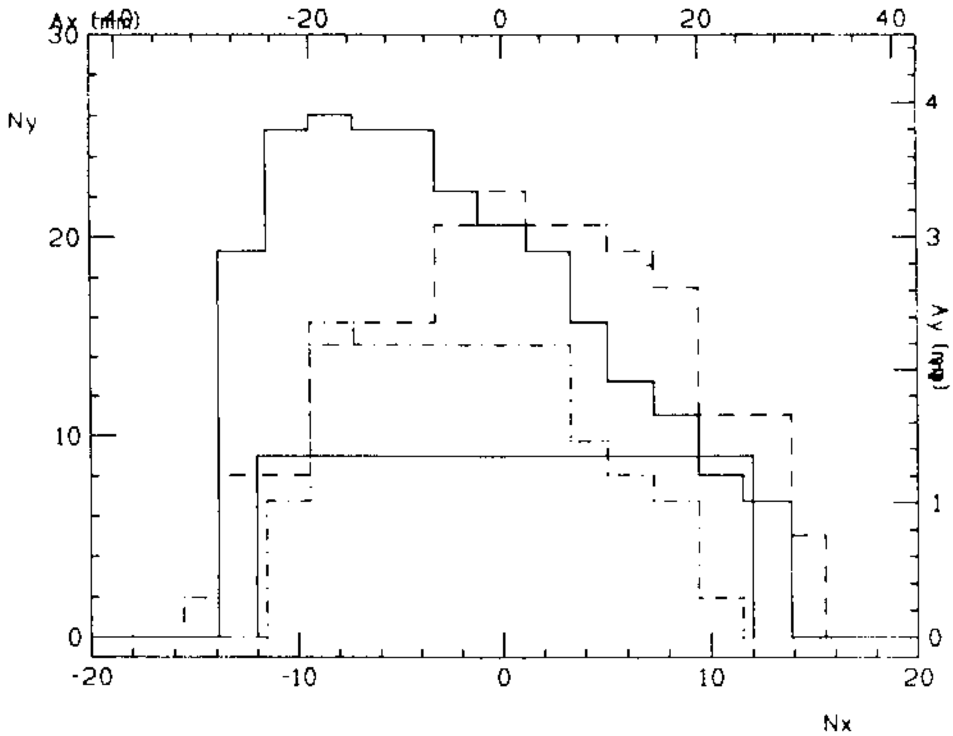

Fig. 4.7 - Dynamic aperture for $\Delta P/P$ = 1% (- - -) and $\Delta P/P$ = -1% (- . - . -), compared with the on energy one and the vacuum chamber aperture (——).

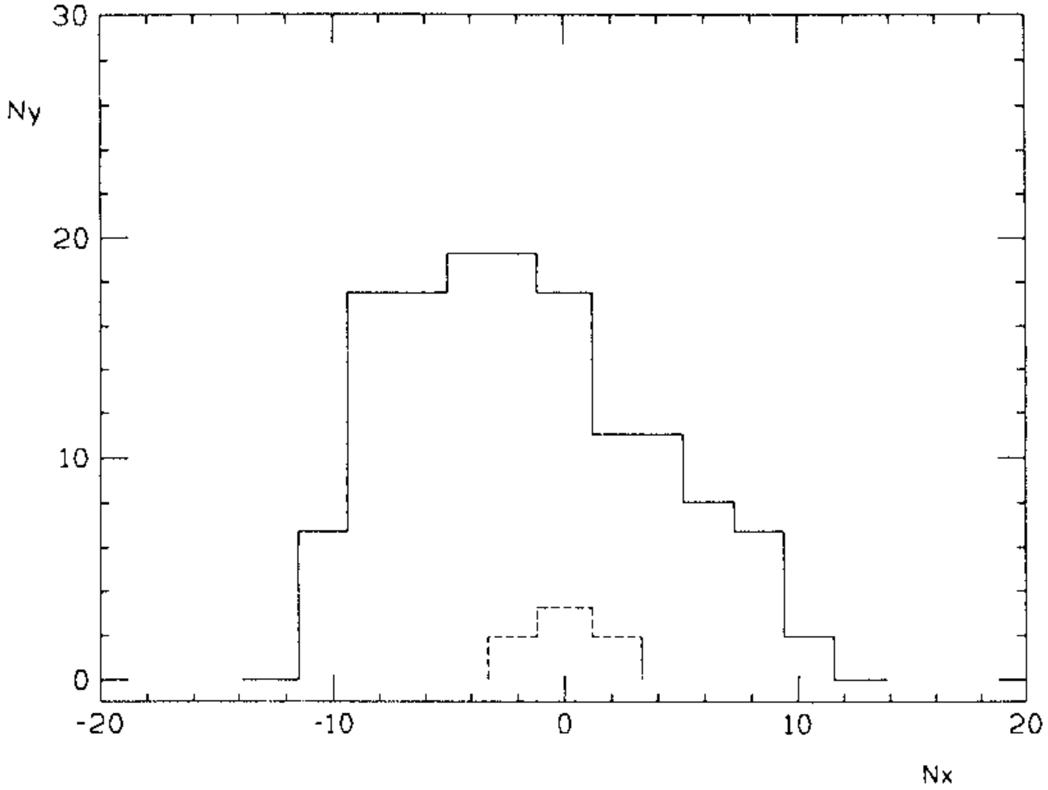

Fig. 4.8 - **Dynamic aperture** for $\Delta P/P = + .7\%$: present lattice (—), previous lattice (- - -).

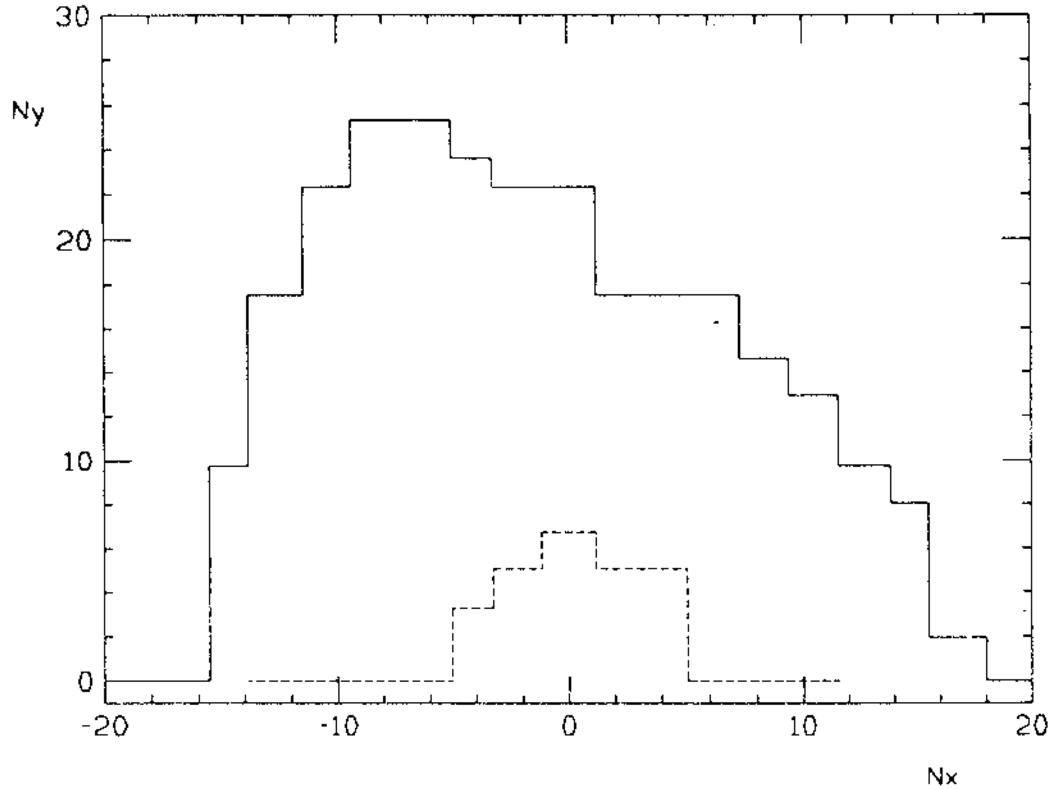

Fig. 4.9 - **Dynamic aperture** for $\Delta P/P = - .7\%$: present lattice (—), previous lattice (- - -).

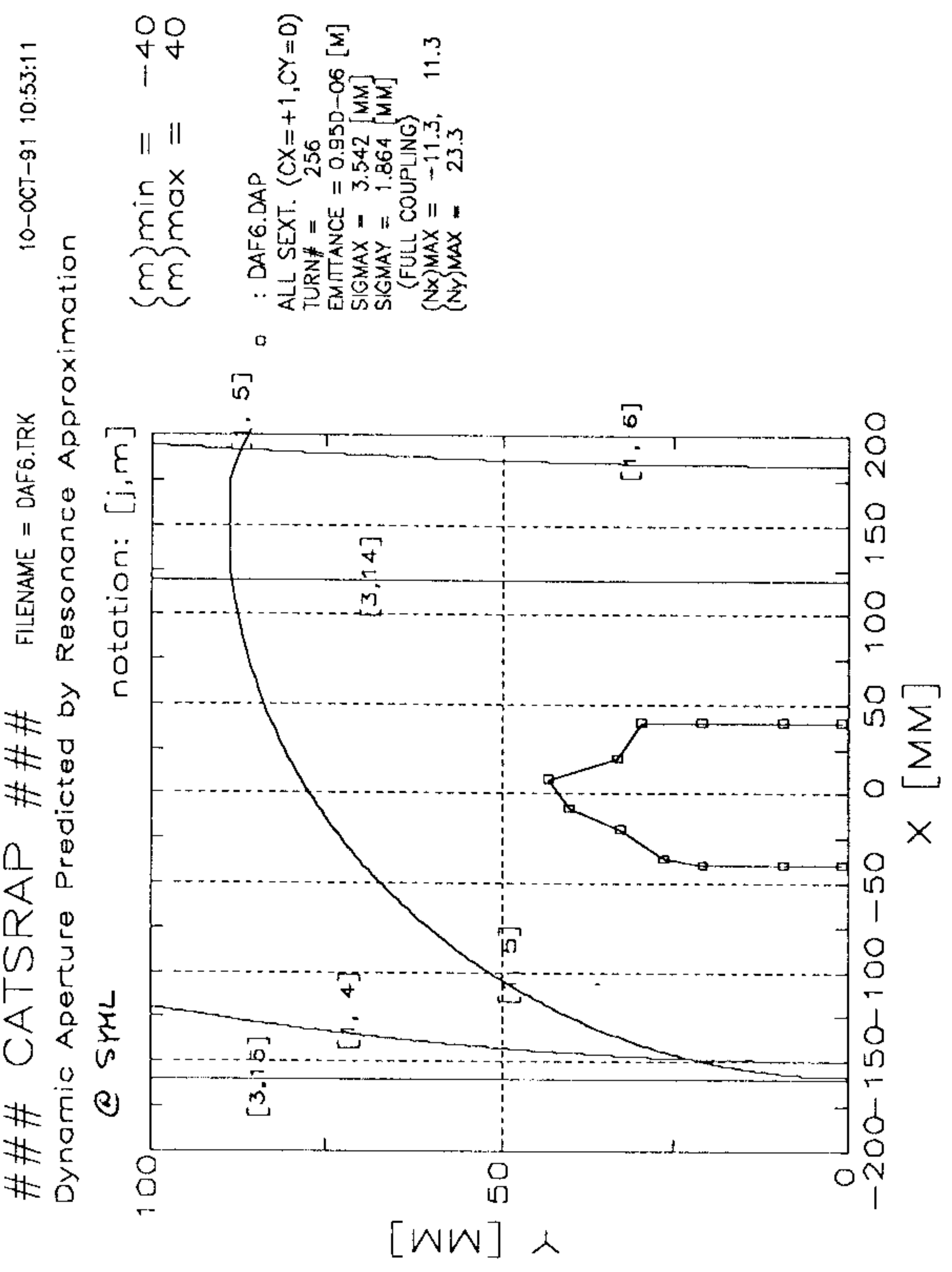

Fig. 4.10 - On energy d**ynamic aperture** at the symmetry point of the ***Long*** (CATS code).

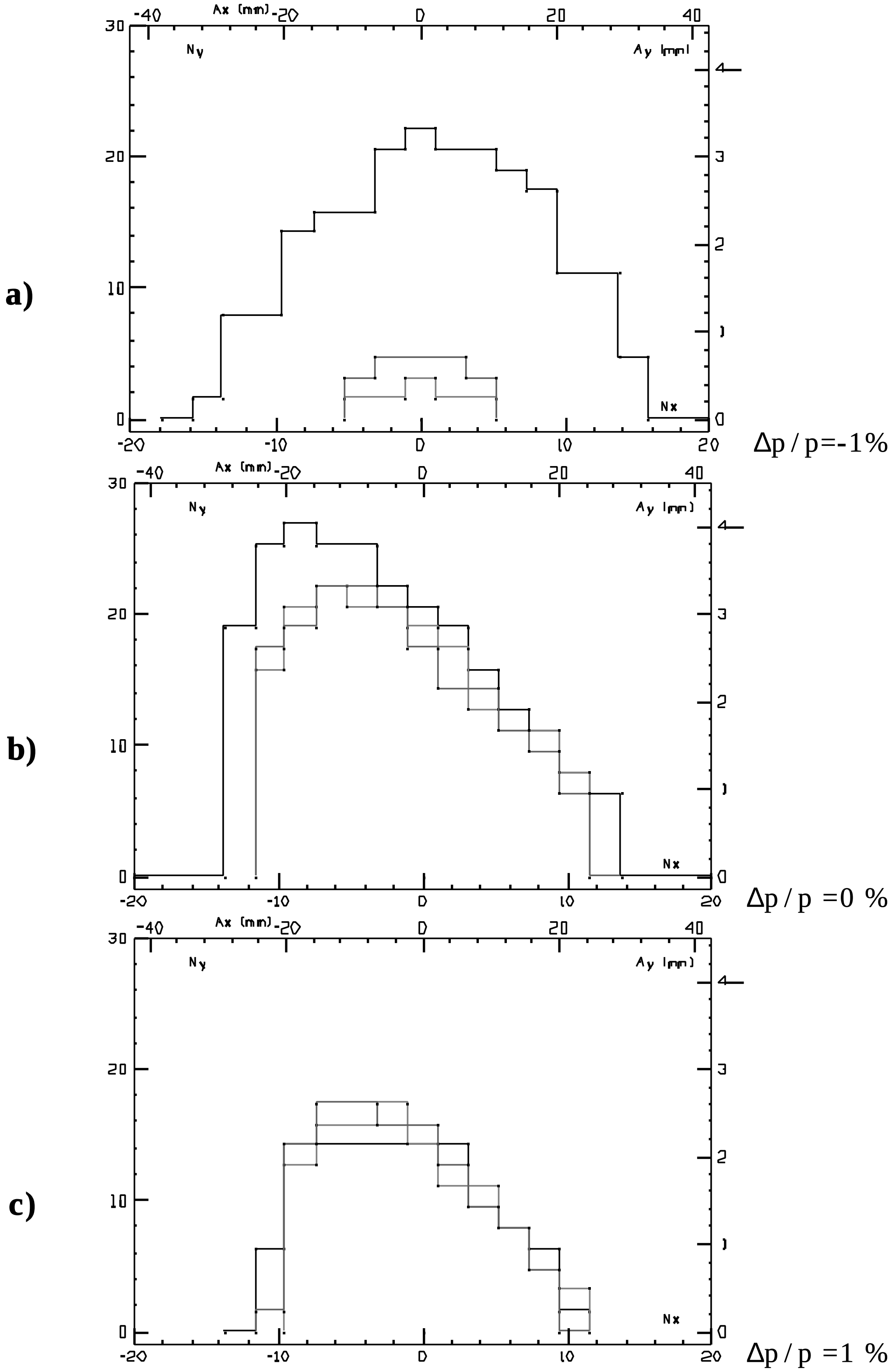

Fig. 5.1 - Dynamic aperture with **dodecapoles in the quadrupoles**.
x off-coupling, y full-coupling.
____ ideal machine, ... dodecapole >0, ---- dodecapole <0.

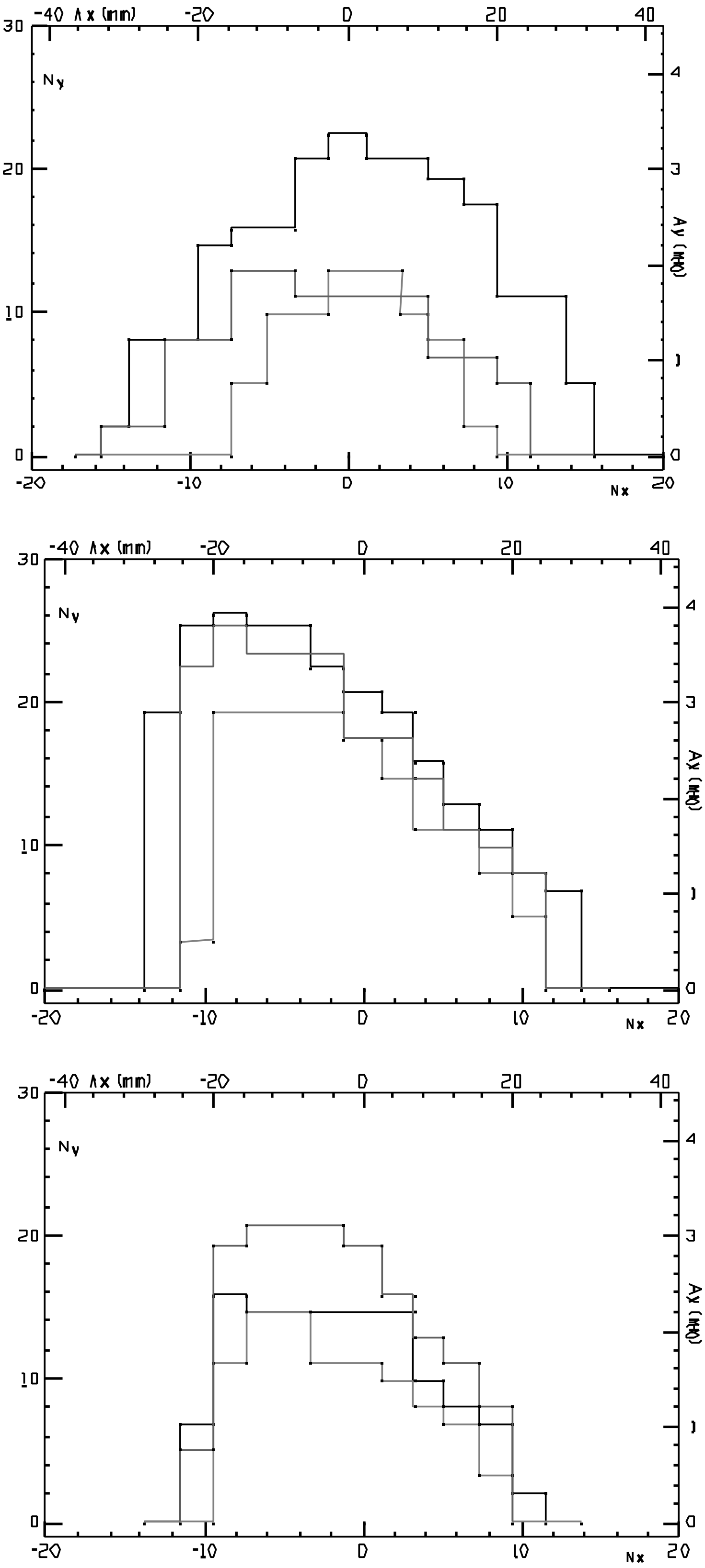

a) $\Delta p / p = -1\%$

b) $\Delta p / p = 0\%$

c) $\Delta p / p = 1\%$

Fig. 5.2 - Dynamic aperture with **sextupoles in dipoles**.
x off-coupling, y full-coupling.
____ ideal machine, ······ sextupole >0, ---- sextupole <0.

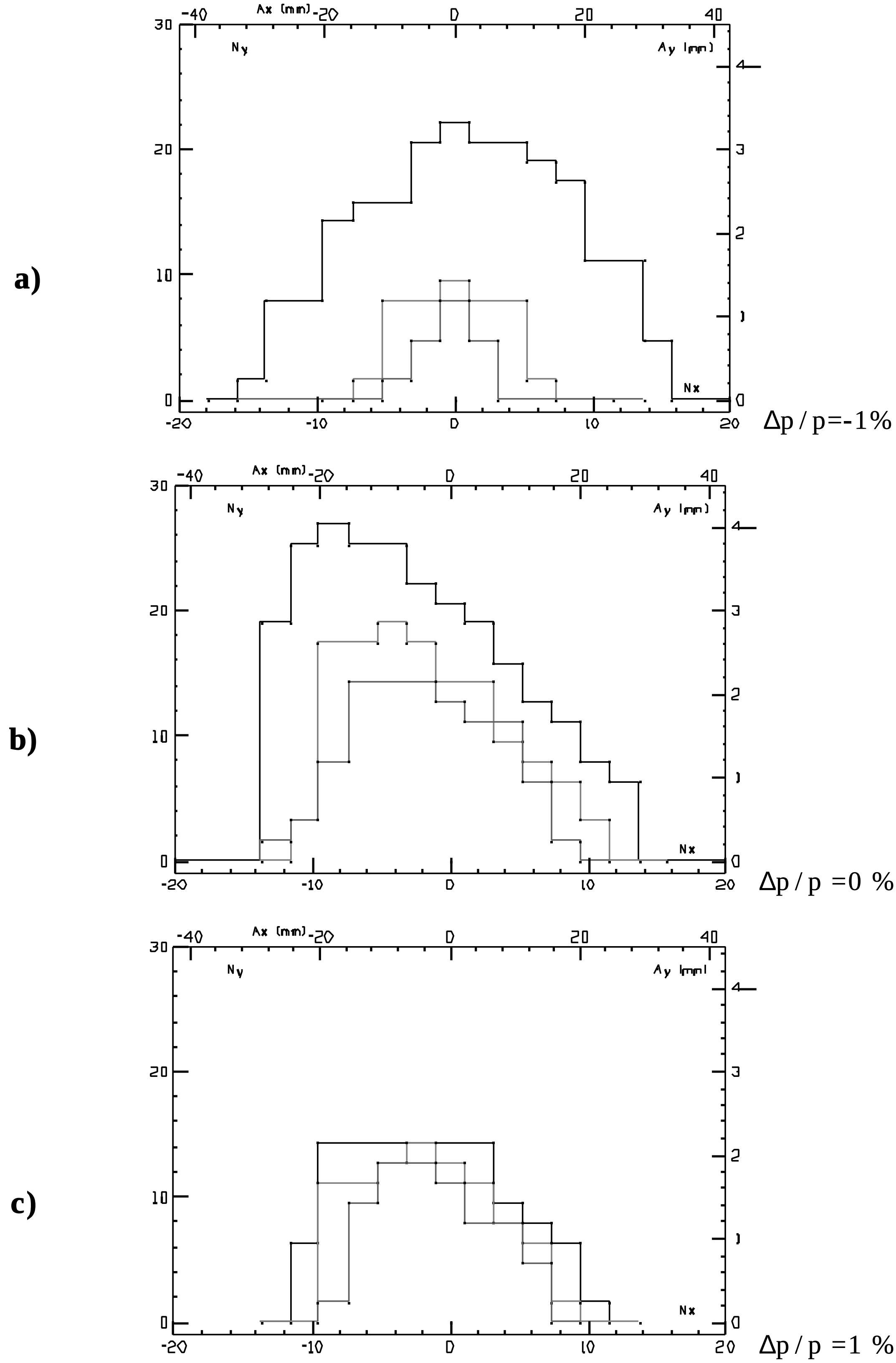

Fig. 5.3 - Dynamic aperture with **decapoles in dipoles**.
x off-coupling, y full-coupling.
—— ideal machine, ······ decapole >0, ---- decapole <0.

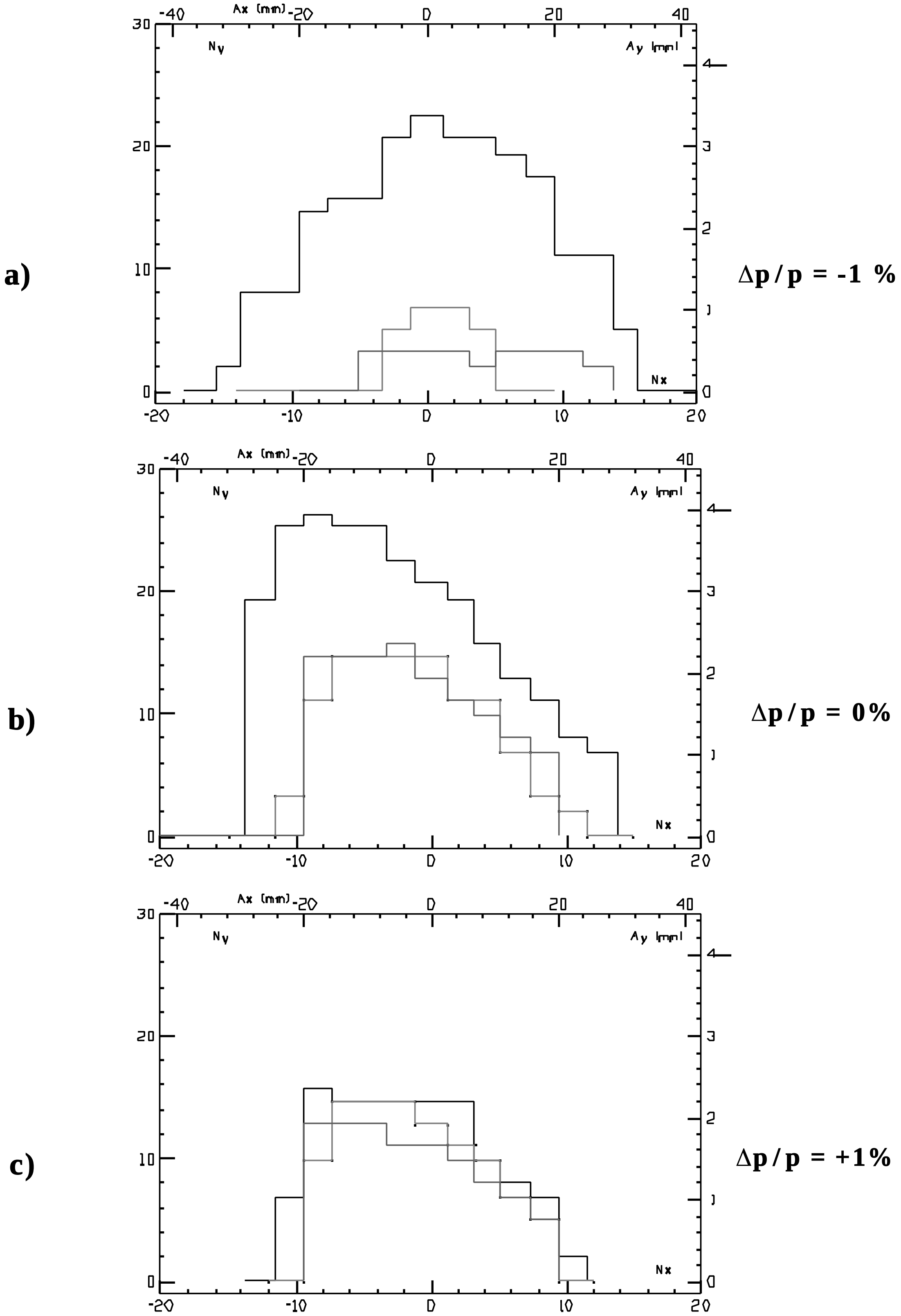

Fig. 5.4 - Dynamic aperture with **dodecapoles in low-β quadrupoles**.
x off-coupling, y full-coupling.
—— ideal machine, .····· dodecapole >0, ---- dodecapole <0.

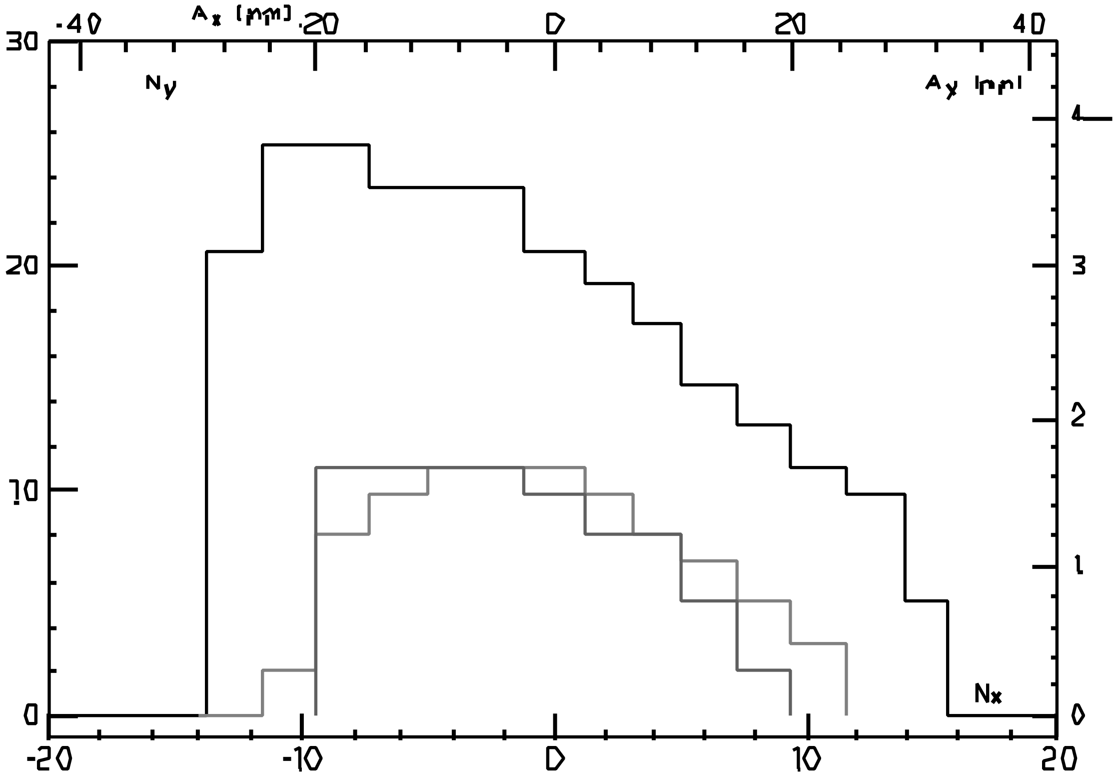

$\Delta p/p$ **= - 0.5 %**

Fig. 5.5 - Dynamic aperture with **dodecapoles in low-β quadrupoles**
for $\Delta P/P$ = -.5%.
x off-coupling, y full-coupling.
——— ideal machine, ... dodecapole >0, ---- dodecapole <0.

a)

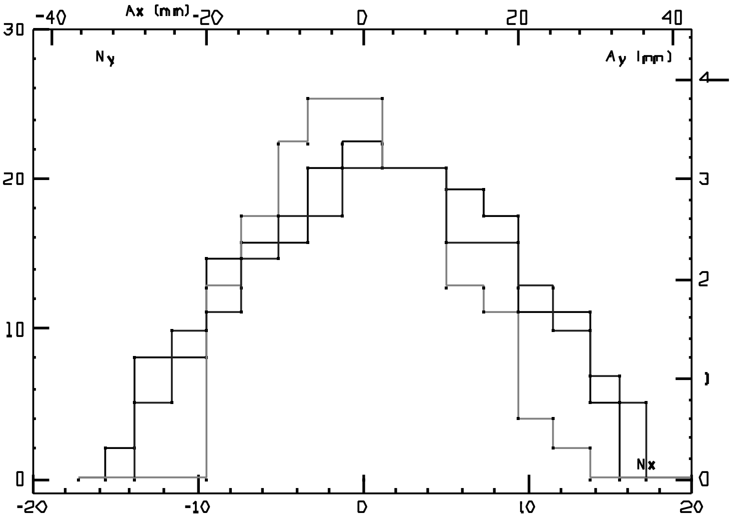

Δp/p = -1. %

b)

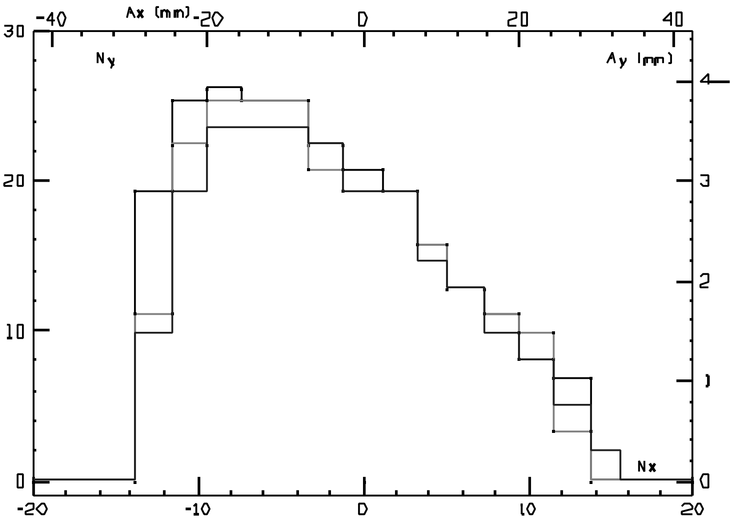

Δp/p = 0 %

c)

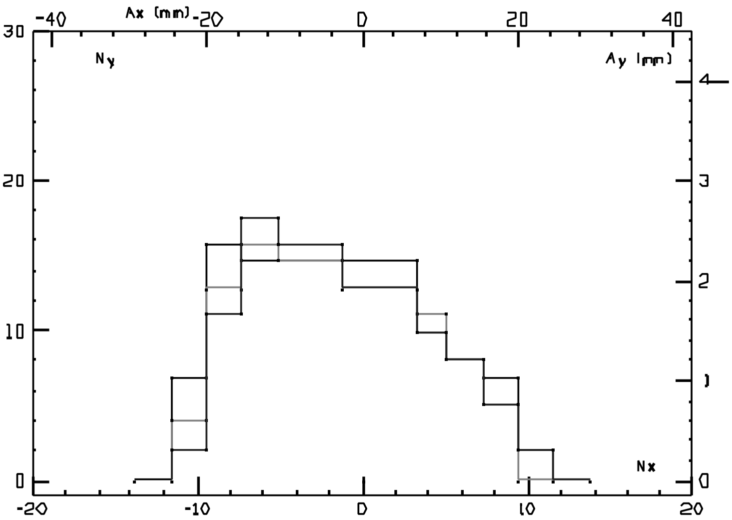

Δp/p = 1. %

Fig. 5.6 - Dynamic aperture with **sextupoles in wigglers**.
x off-coupling, y full-coupling.
—— ideal machine, ... sextupole >0, ---- sextupole <0.

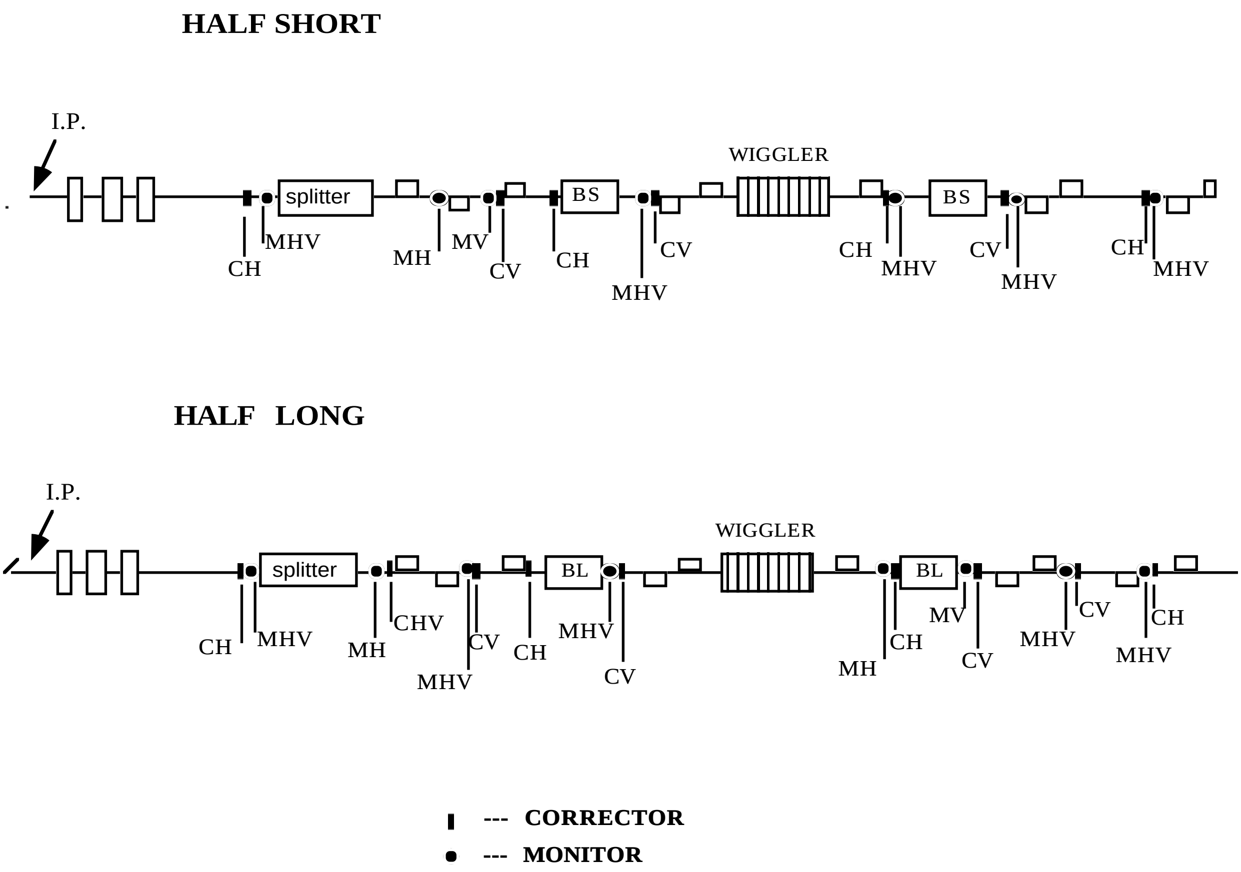

Fig. 6.1 - Arrangement of monitors and correctors in half of the ***Short*** and ***Long*** section.

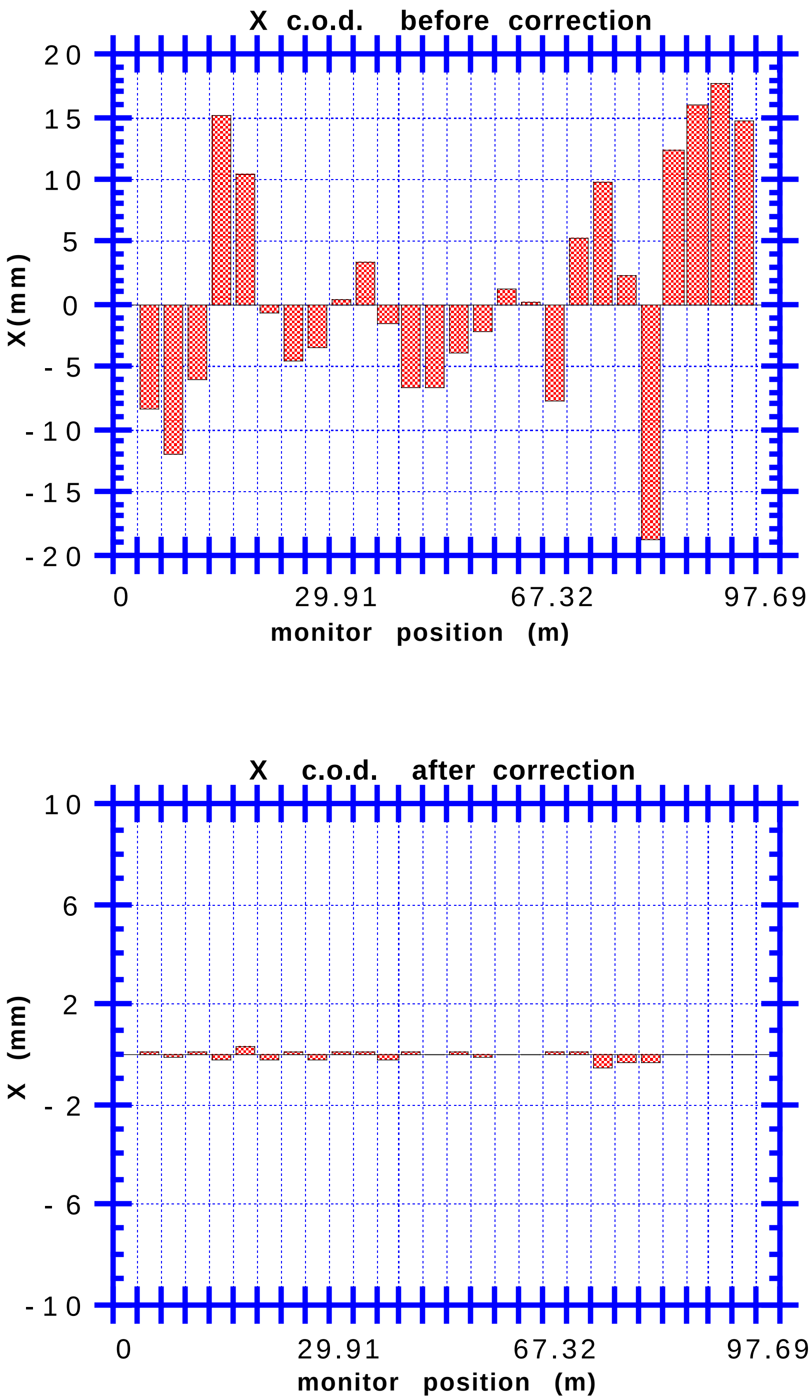

Fig. 6.2 - Horizontal closed orbit amplitude at the monitors before and after correction.

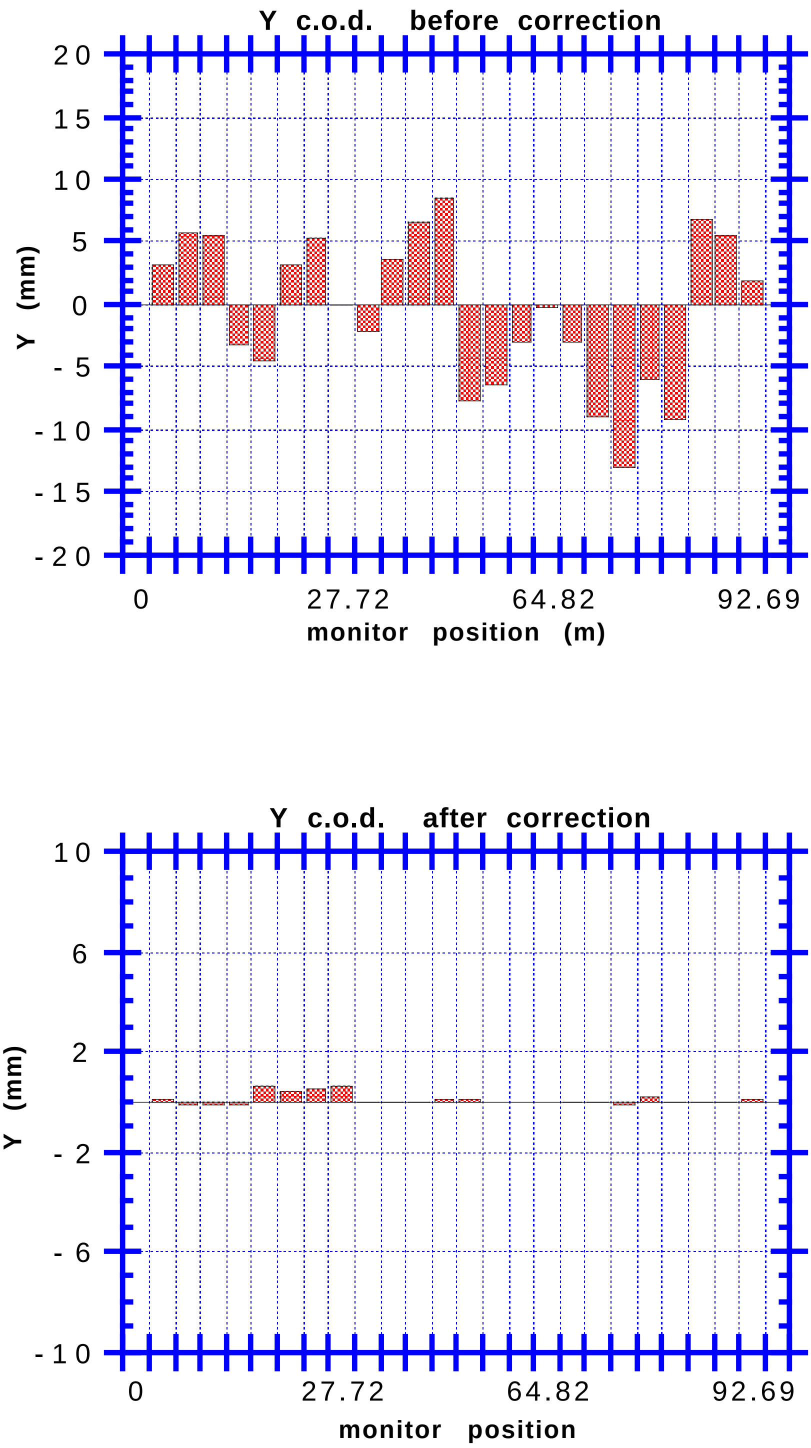

Fig. 6.3 - Vertical closed orbit amplitude at the monitors before and after correction.

a)

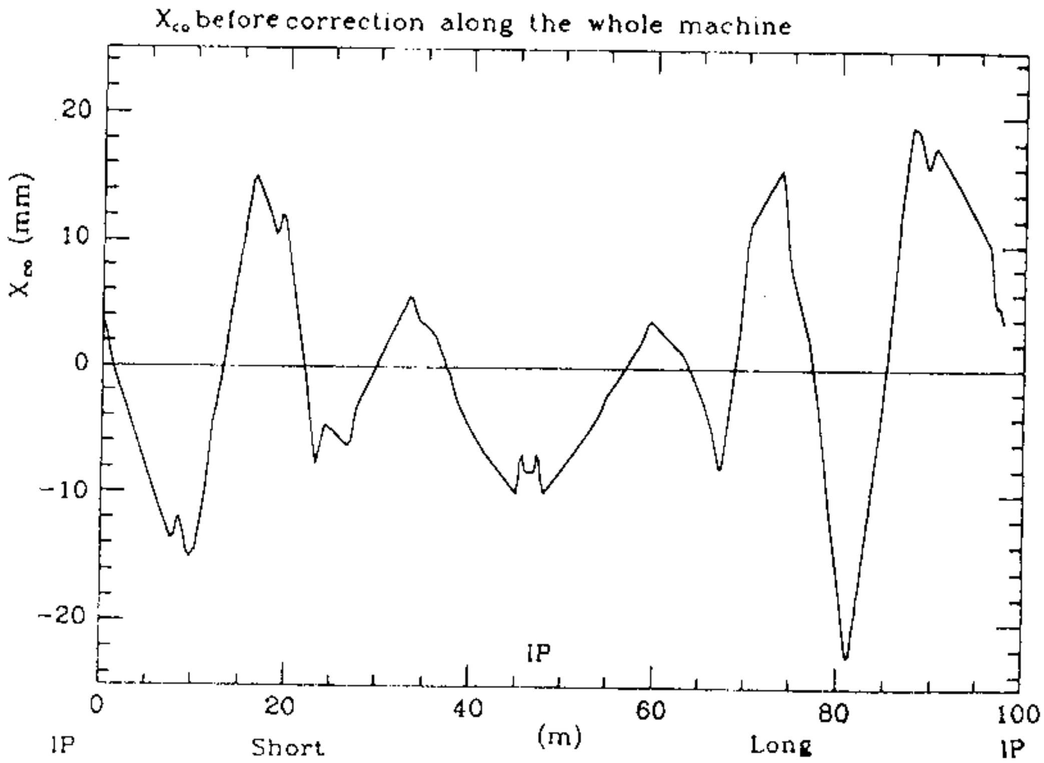

b)

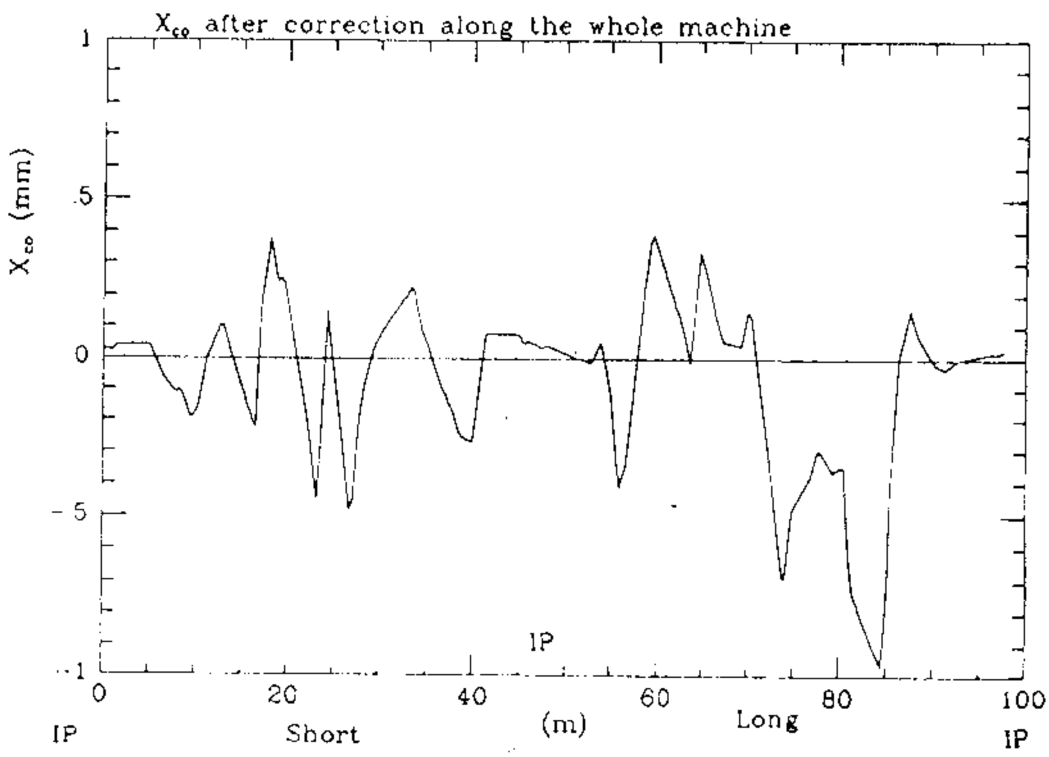

Fig. 6.4 - Graphic of a sample closed orbit along the whole machine in the **horizontal plane**: a) before correction; b) after correction.

a)

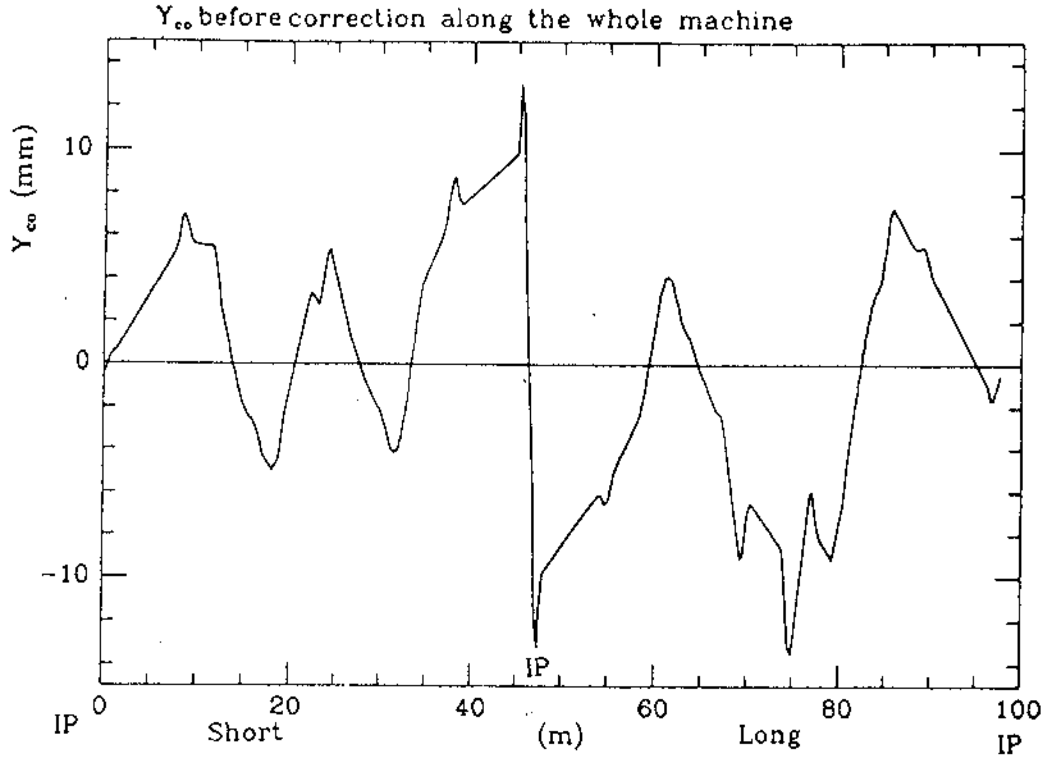

b)

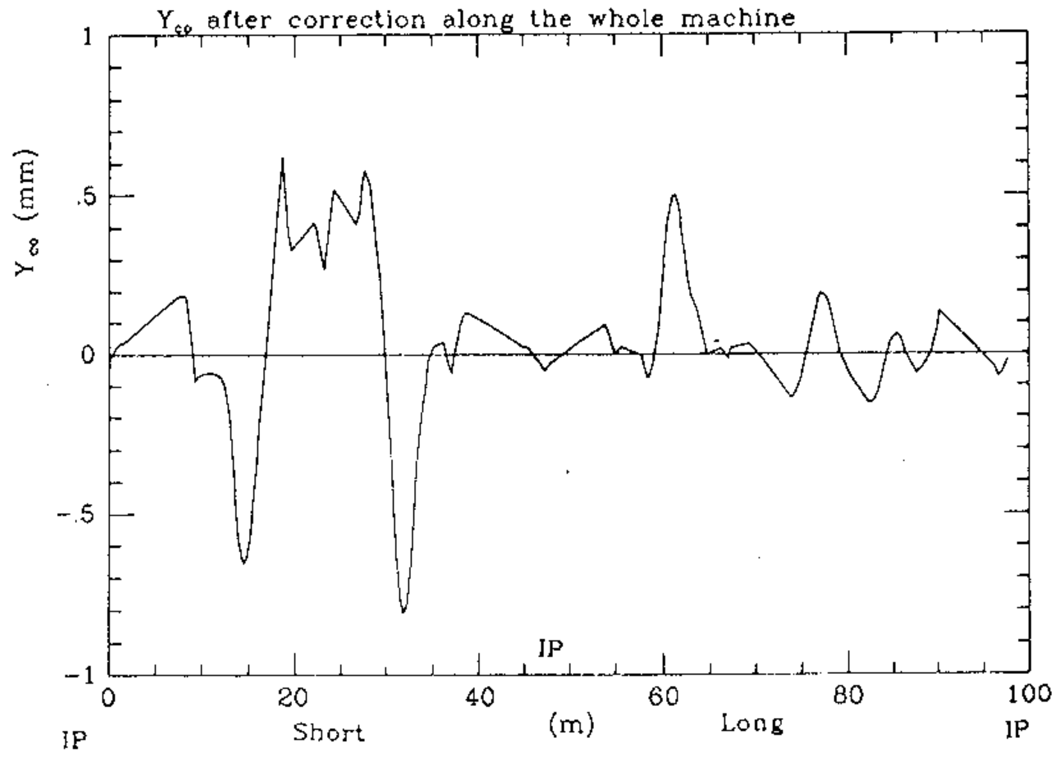

Fig. 6.5 - Graphic of a sample closed orbit along the whole machine in the **vertical plane**: a) before correction; b) after correction.

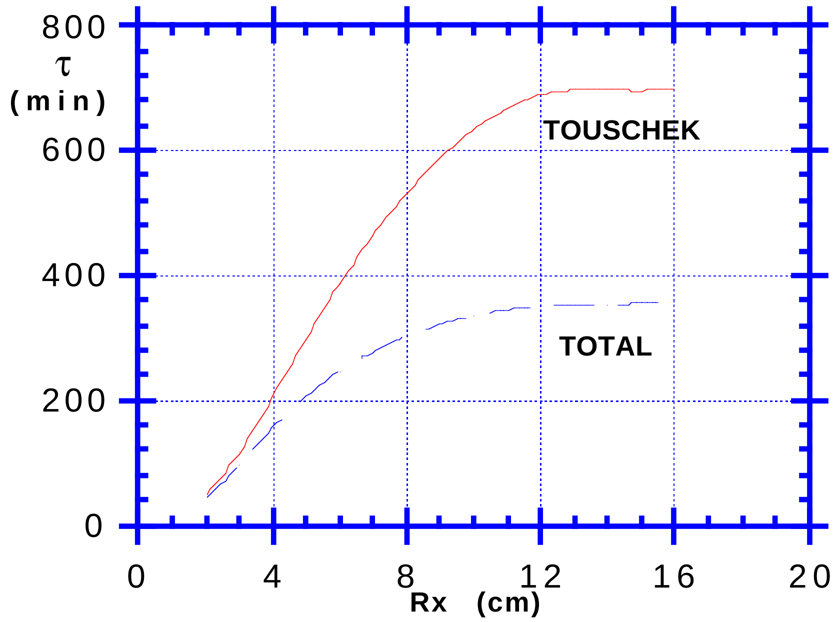

Fig. 7.1 - Touschek and total beam lifetime as a function of the vacuum chamber half-aperture.

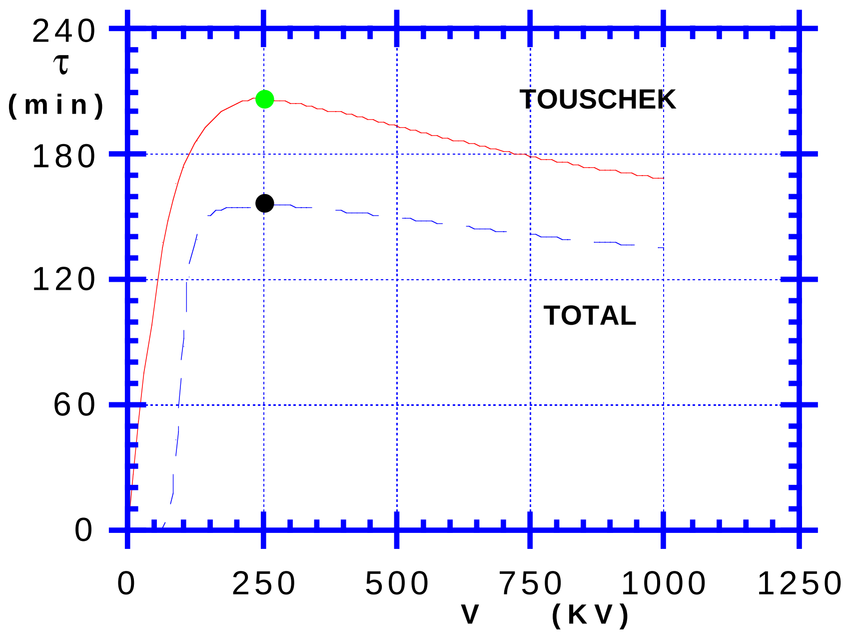

Fig. 7.2 - Touschek and total beam lifetime as a function of the R.F. voltage.

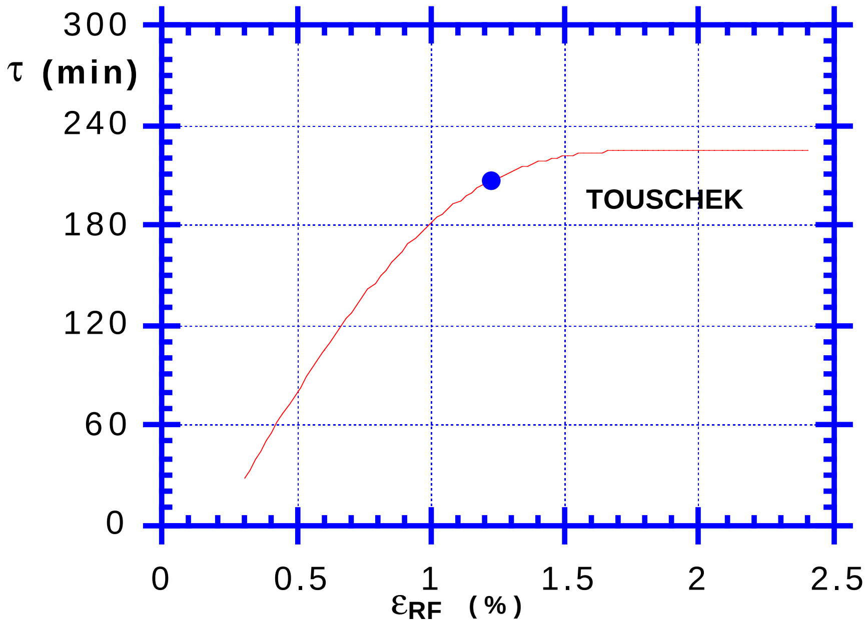

Fig. 7.3 - Touschek and total beam lifetime as a function of R.F. acceptance for a fixed bunch length (σ_z = 3 cm).

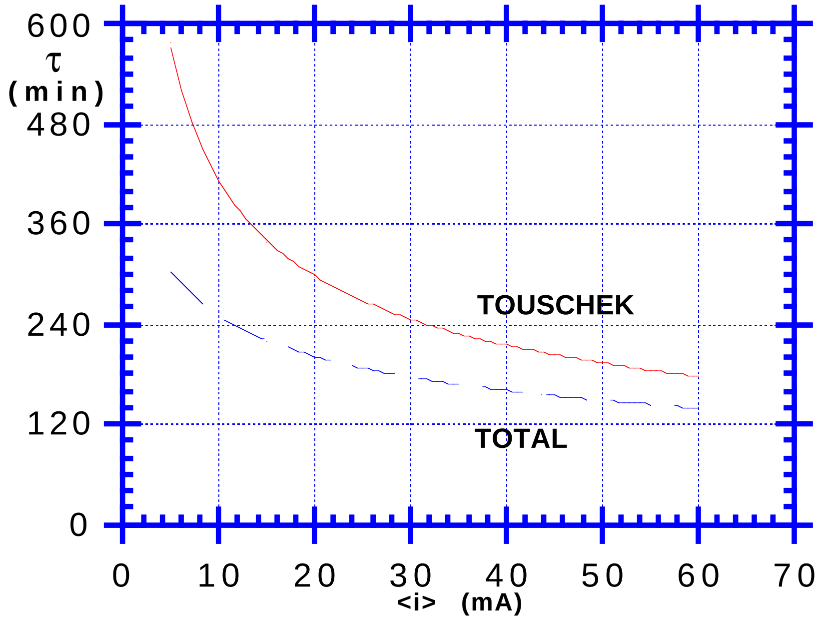

Fig. 7.4 - Touschek and total beam lifetime as a function of the average bunch current.

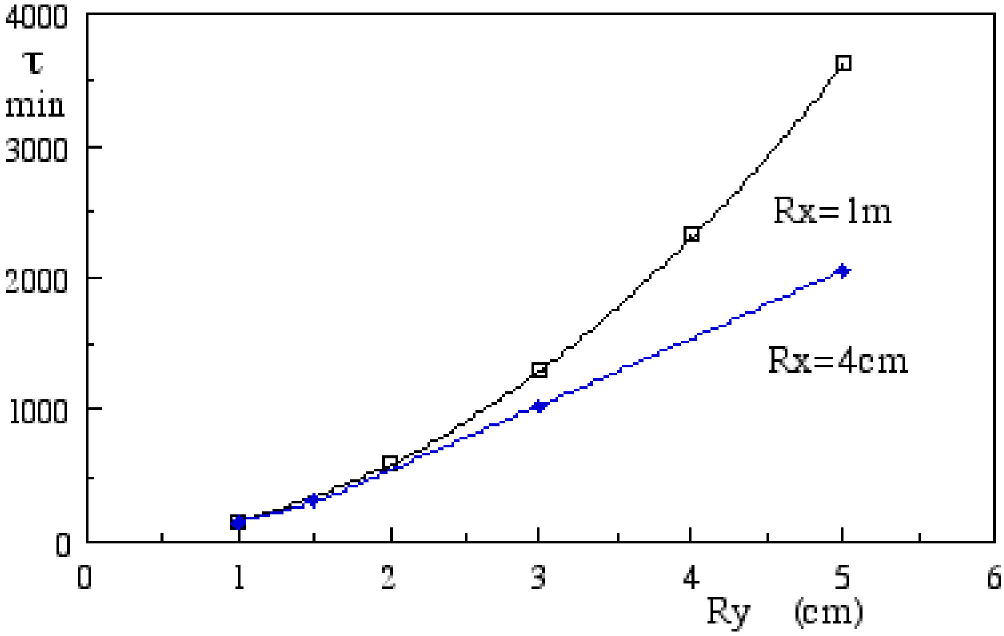

Fig. 7.5 - Gas scattering beam lifetime as a function of the vertical vacuum chamber half-aperture for different values of the horizontal half aperture R_x.

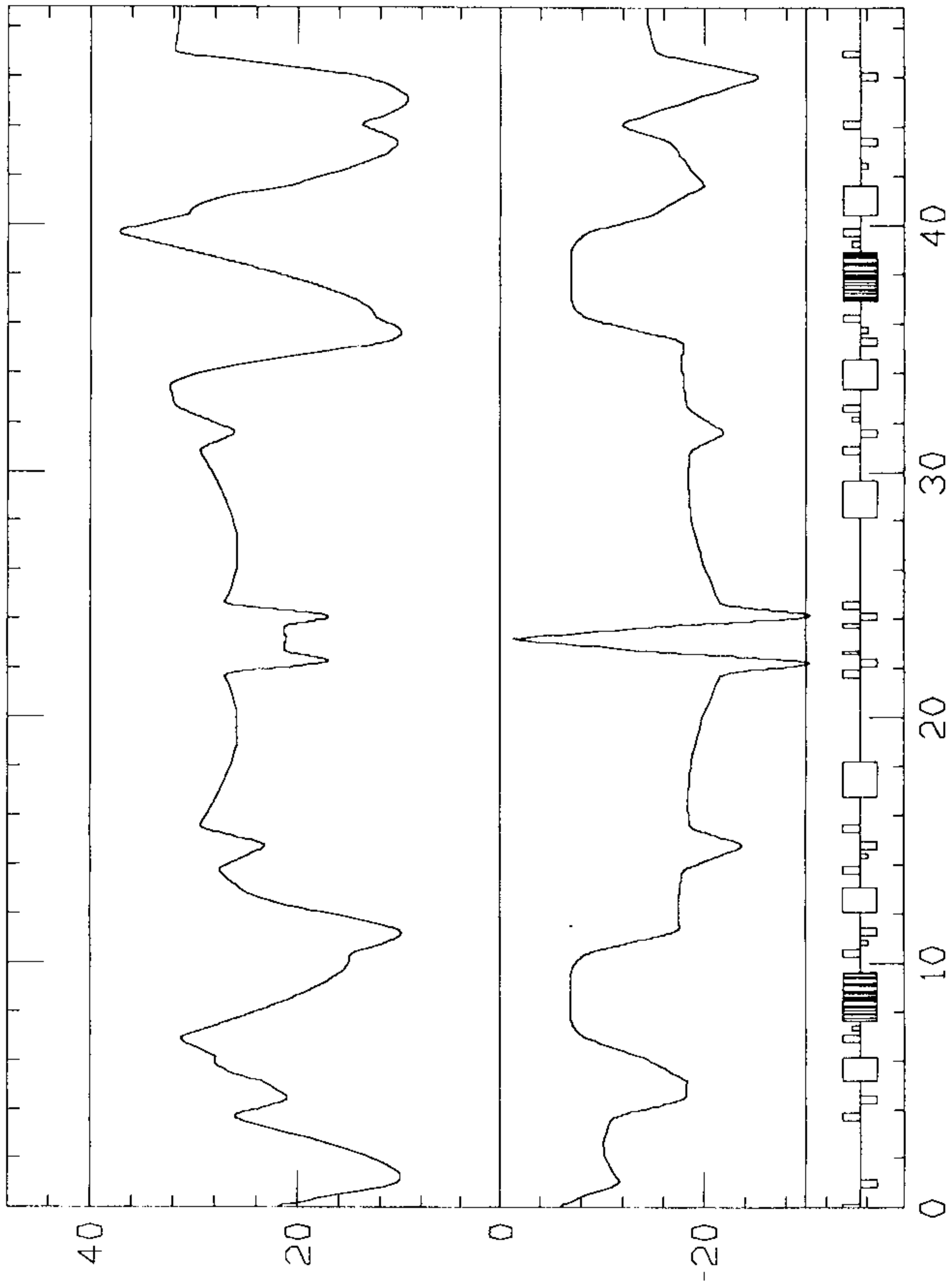

Fig. 7.6- Beam envelope along the machine for: 10 σ_x (off-coupling), 10 σ_p, 9 σ_y (full-coupling).

APPENDIX

In this Appendix a summary of some of the lattices studied for DAΦNE is presented. All of them have four quadrupoles in the insertion of the *Long* (8 in total in the injection section), and the same total tunes. The horizontal tune difference between *Short* and *Long* has been kept constant. The *Short* lattice has been kept fixed and only the quadrupole strengths varied in order to change the vertical tune, to fit the total tune.

In **Table A.1** the main differences in the *Long* are summarized: the lattice described in detail in this note is called DAF6, the other five are different in the focusing of the last four quadrupole, in the relative drift lengths between them and then in the optical functions behaviour.

Table A.1

	DAF6	DAF6B	DAF7	DAF8	DAF4	DAF5
FOCUSING	DFDF	DFDF	DFDF	FDFD	DFDF	FDFD
NUY SHORT	2.59	2.59	2.59	2.59	2.62	2.62
NUY LONG	2.26	2.26	2.26	2.26	2.23	2.23
CHROM. X	-6.90	-6.70	-6.31	-5.06	-6.84	-6.35
CHROM. Y	-16.95	-16.94	-16.94	-20.60	-16.43	-17.18
BETAX SYML (m)	13.20	10.40	4.20	1.90	1.40	4.50
BETAY SYML (m)	7.30	7.10	6.70	7.30	10.90	8.40
DX SYML (m)	-0.99	-0.88	-0.56	-0.37	-0.32	-0.58
BETAY MAX (m)	18.60	18.40	17.90	13.90	11.60	21.40
QL4 (m-2)	-1.130138	-1.032482	-0.557422	2.687374	1.918675	-0.378425
QL3 (m-2)	3.971584	3.796281	3.242549	-2.913116	-2.113557	3.193222
QL2 (m-2)	-2.636017	-2.680664	-2.956853	3.272624	3.298401	-2.962232
QL1 (m-2)	2.354521	2.390960	2.538772	-1.166577	-1.571374	2.521506
L3 (m)	1.90	1.80	1.30	1.00	1.30	1.30
L5 (m)	1.40	1.50	2.00	2.30	2.00	2.00
QS4 (m-2)	-1.956186	-1.956186	-1.956186	-1.956186	-1.955816	-1.955816
QS3 (m-2)	2.411140	2.411140	2.411140	2.411140	2.417252	2.417252
QS2 (m-2)	-3.084065	-3.084065	-3.084065	-3.084065	-3.305633	-3.305633
QS1 (m-2)	3.981571	3.981571	3.981571	3.981571	4.053376	4.053376

For each lattice we list the focusing type of the quadruplet, the vertical tunes (*Short* and *Long*), the absolute chromaticities, the values of $\beta_{x,y}$ and D_x at the symmetry point of the *Long*, the maximum β_y after the last bending, the quadrupole strengths (positive for focusing and negative for defocusing) - for the *Long* and *Short* - and finally the two drift lengths used to tune the optical functions.

Briefly, we note that:

- out of six lattices, four have a difference $\Delta\nu_y$ of .33 and the last two have $\Delta\nu_y = .39$;
- the high β_y after the last bending, as in some of the lattices listed, may be useful to insert a scraper in order to reduce the background in the interaction point;
- Touschek lifetime calculations have shown that a high β_x at the injection section is not dangerous.

The optical functions of the *Long* for the five lattices are plotted in **Figs. A.1** to **A.5**, and in **Fig. A.6** are shown the optical functins of the *Short* with different vertical tune ($\nu_y = 2.62$).

For comparison, the on-energy dynamic apertures of all the lattices have been computed with the same sextupole configuration as in Table 4.I, and are presented in **Figs. A.7** to **A.11**.

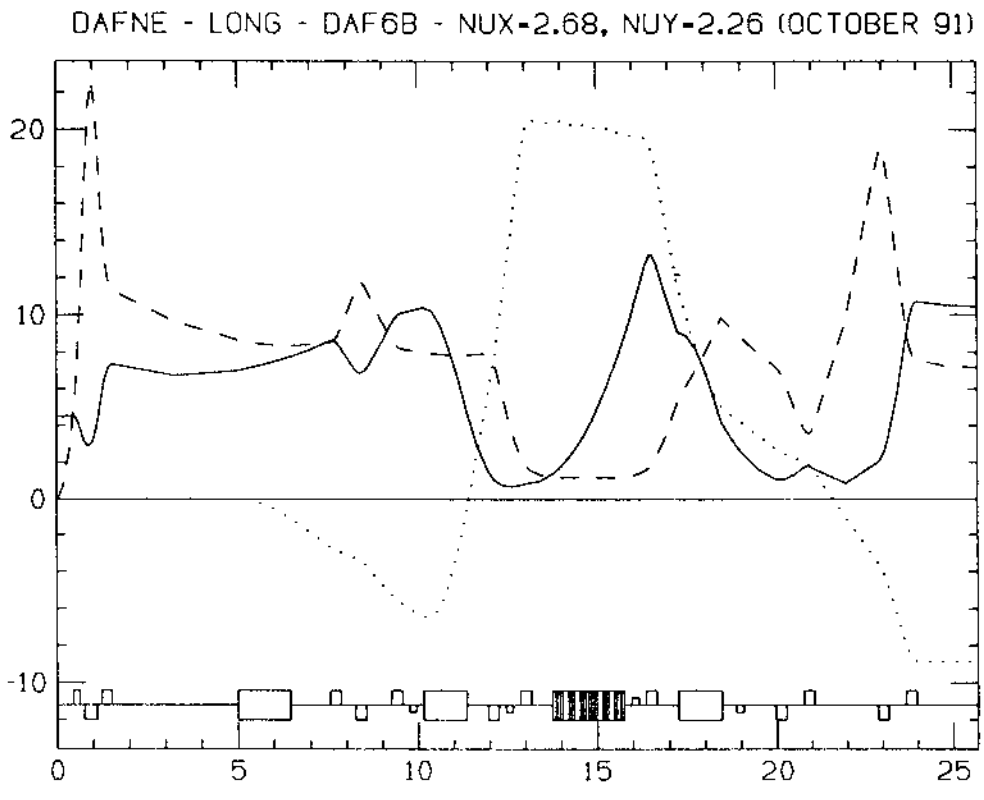

Fig. A.1 - ***Long*** lattice optical functions for DAF6B.

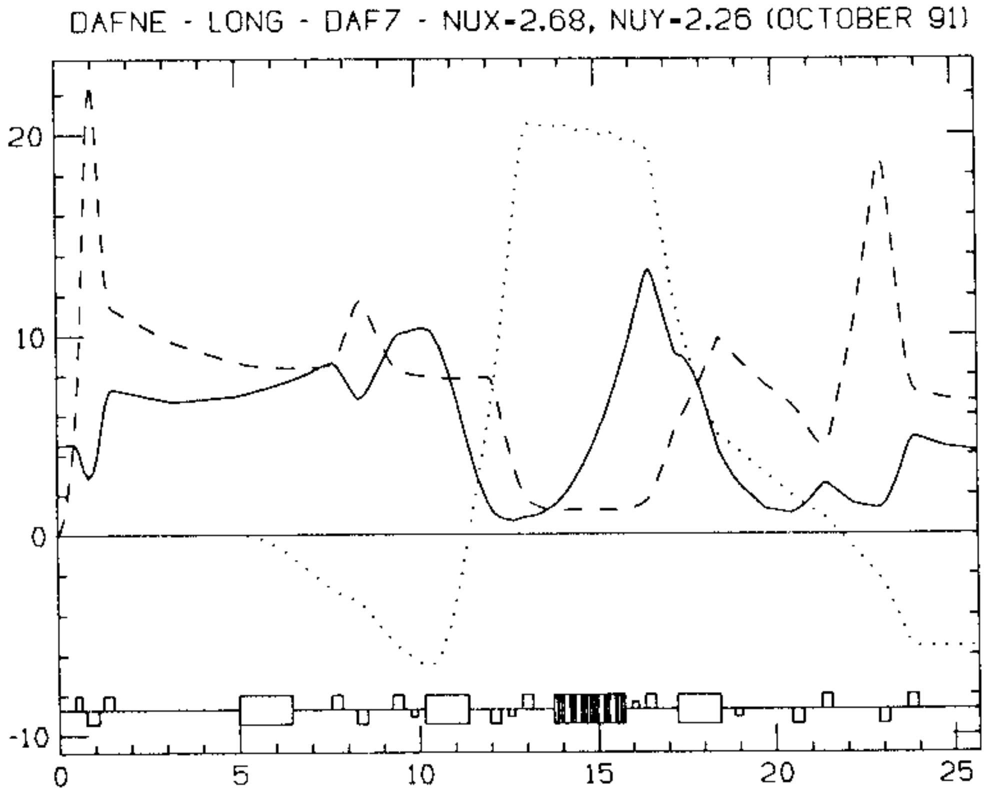

Fig. A.2 - ***Long*** lattice optical functions for DAF7.

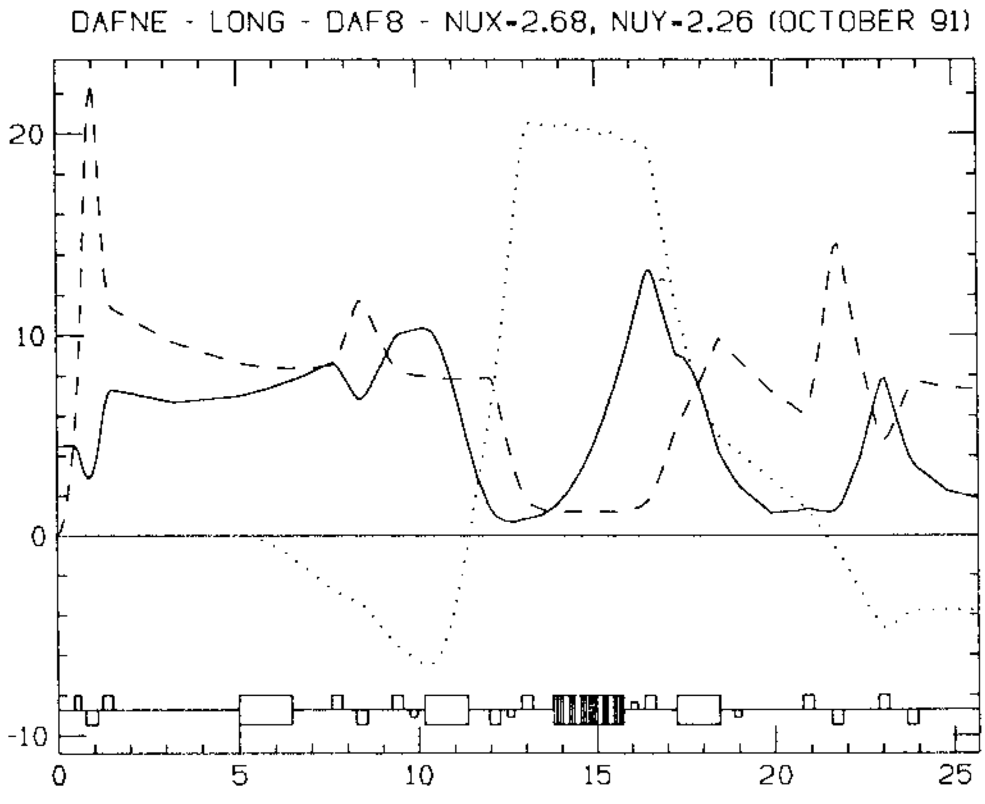

Fig. A.3 - ***Long*** lattice optical functions for DAF8.

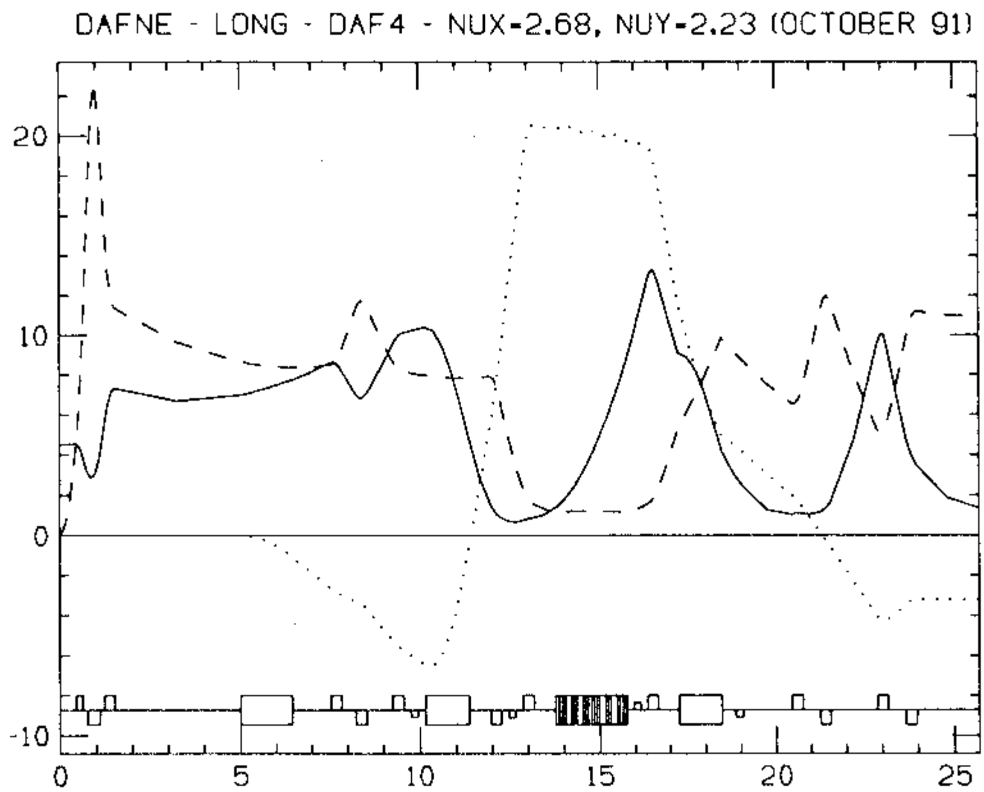

Fig. A.4 - ***Long*** lattice optical functions for DAF4.

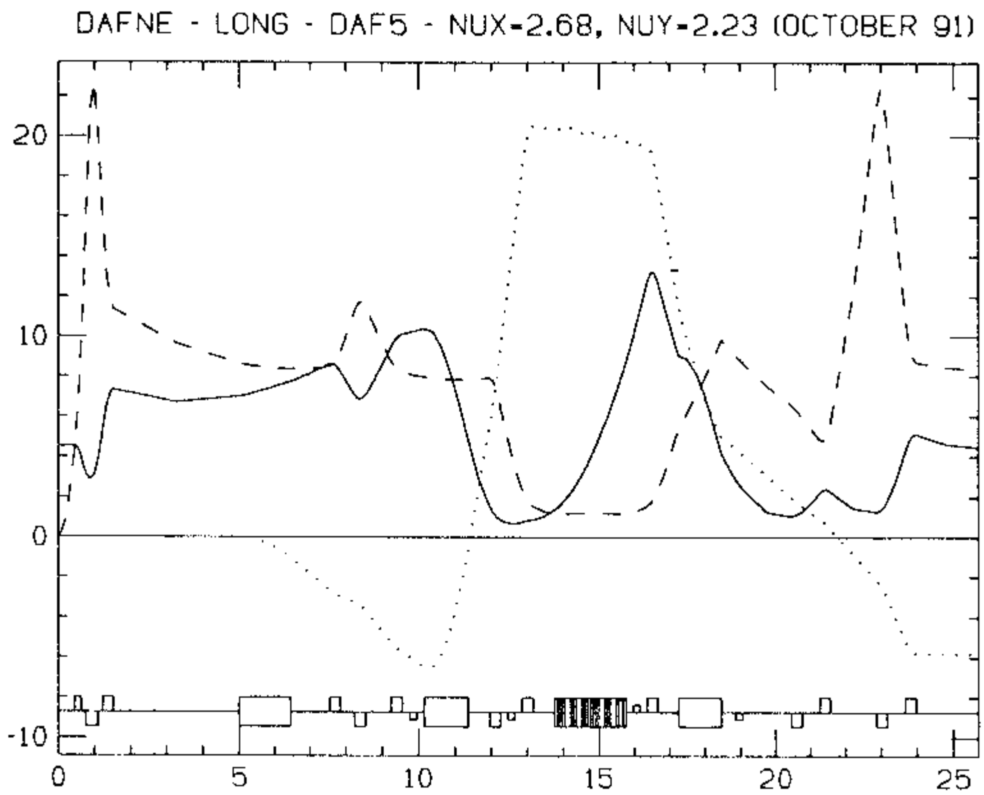

Fig. A.5 - ***Long*** lattice optical functions for DAF5.

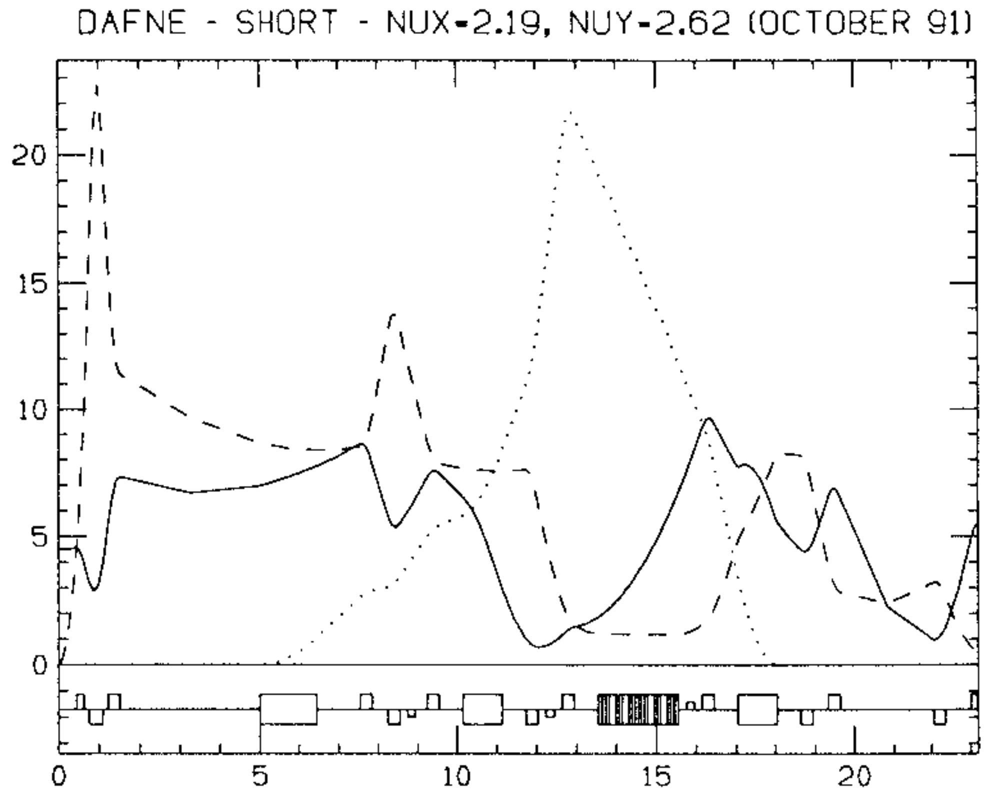

Fig. A.6 - ***Short*** lattice optical functions for DAF4 and DAF5.

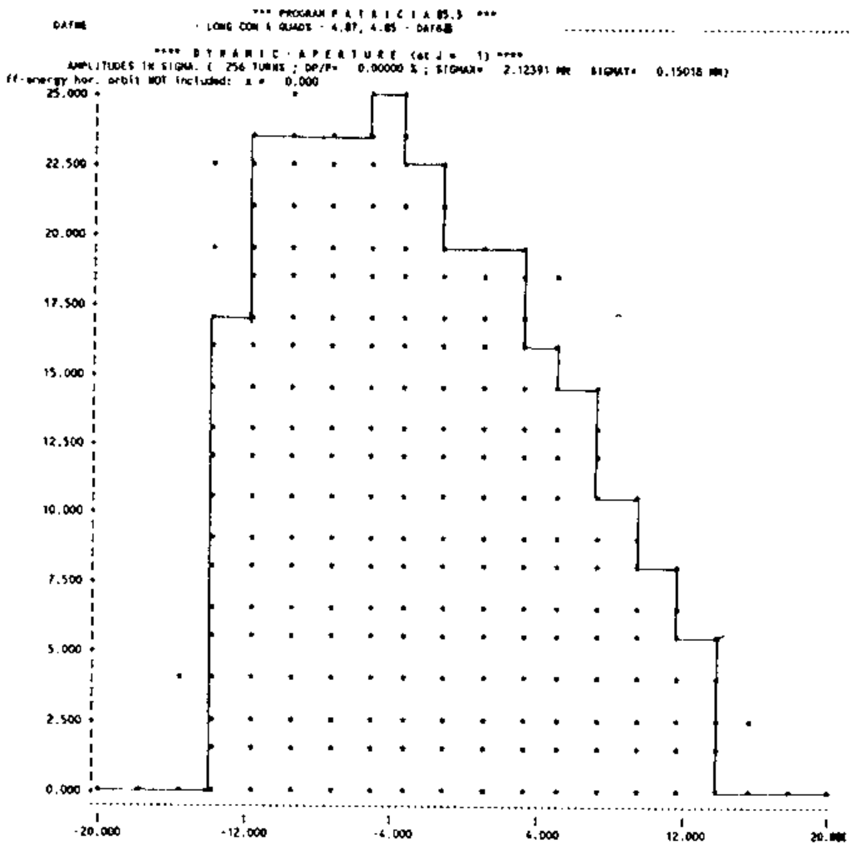

Fig. A.7 - DAF6B dynamic aperture.

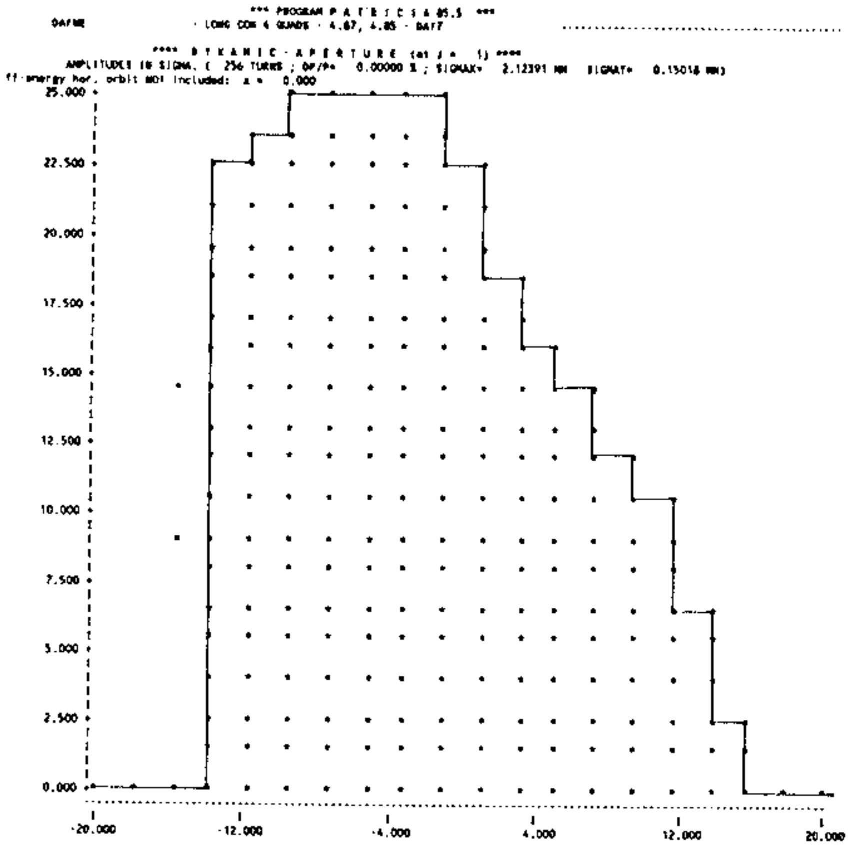

Fig. A.8 - DAF7 dynamic apertur.

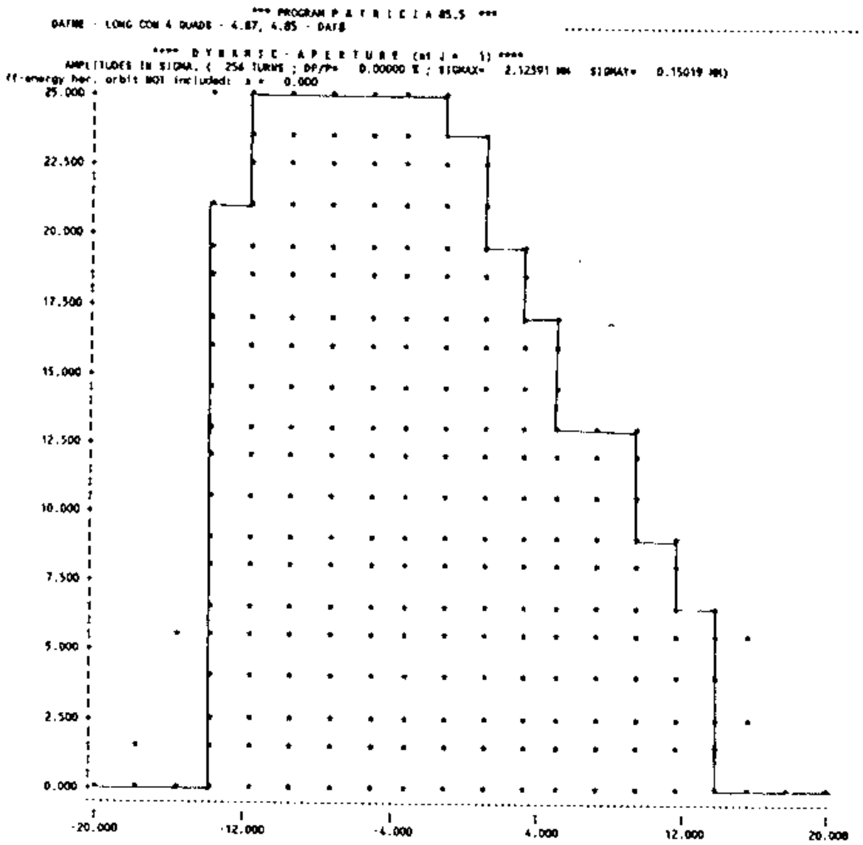

Fig. A.9- DAF8 dynamic aperture.

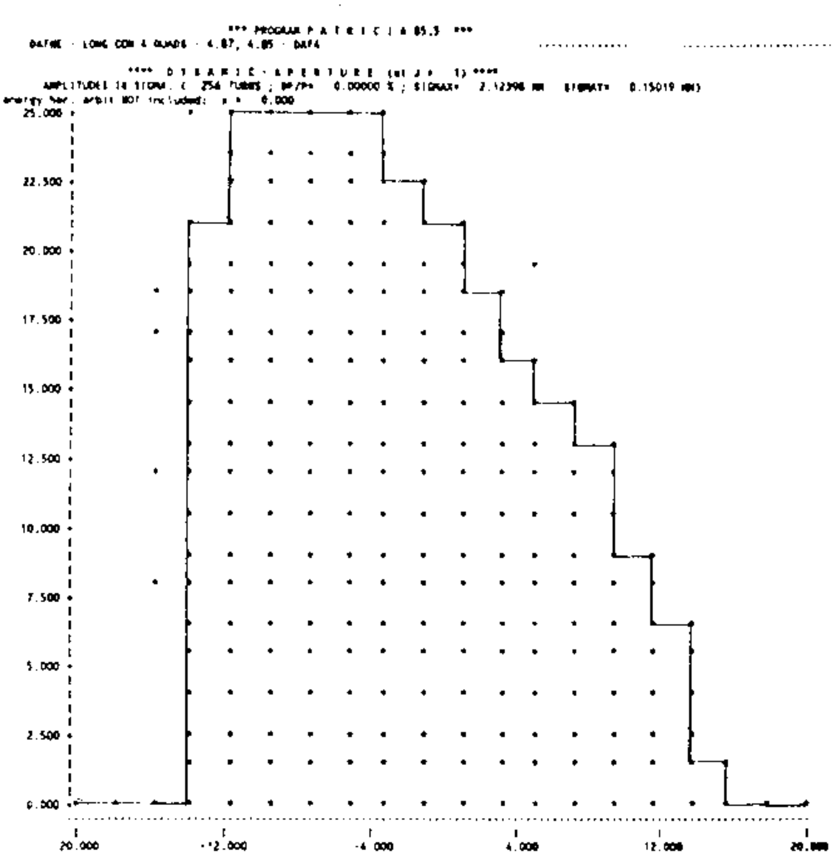

Fig. A.10 - DAF4 dynamic aperture.

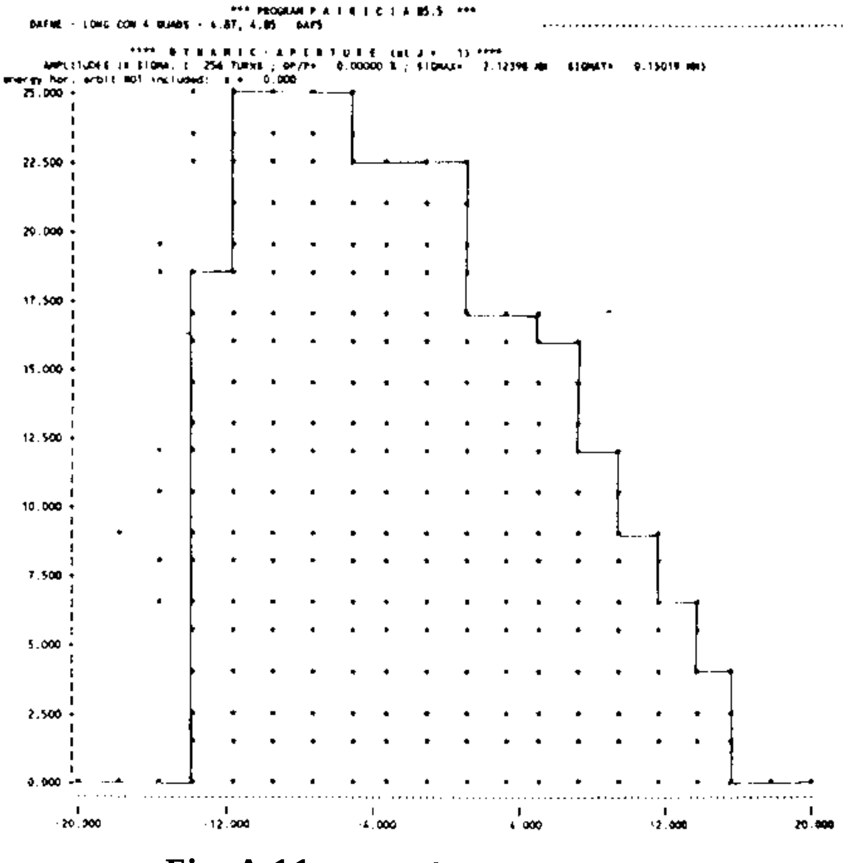

Fig. A.11 - DAF5 dynamic aperture.